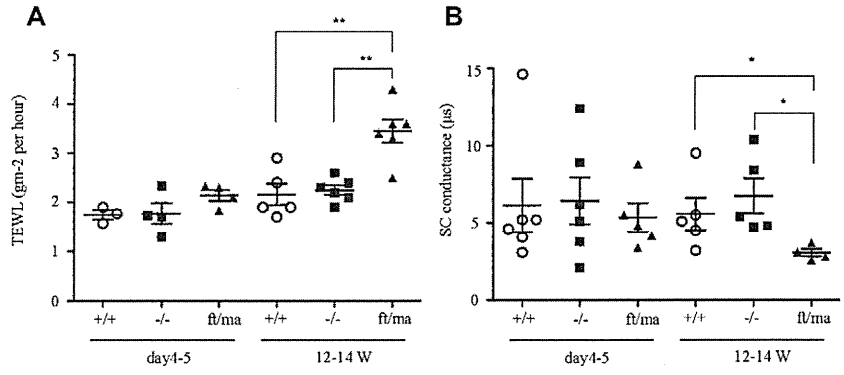

FIG E3. Comparison of TEWL **(A)** and SC hydration **(B)** between P4 and P5 and 12- to 14-week-old wild-type *(+/+)*, *Flg*$^{-/-}$ *(−/−)*, and ft/ma mice in a steady state under normal unmanipulated housing conditions. At 12 to 14 weeks, the ft/ma mice used in this study had spontaneous dermatitis. **P* < .05 and ***P* < .01.

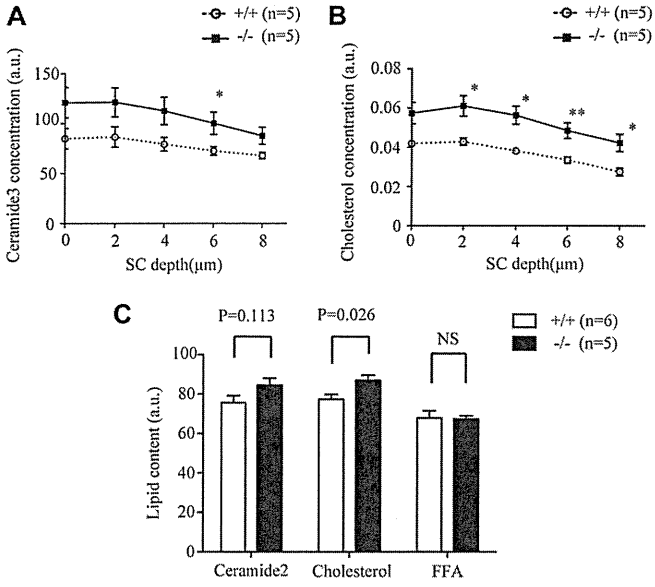

FIG E4. Comparison of SC lipid contents between neonatal wild-type *(+/+)* and *Flg*$^{-/-}$ *(−/−)* mice. **A** and **B,** Dorsal skin ceramide 3 (Fig E4, *A*) and cholesterol (Fig E4, *B*) profiles were measured by using *in vivo* confocal Raman microspectroscopy. **C,** Analysis of lipid extracts isolated from SC sheets. *FFA,* Free fatty acids; *NS,* not significant. **P* < .05 and ***P* < .01.

nature immunology

Stress-induced production of chemokines by hair follicles regulates the trafficking of dendritic cells in skin

Keisuke Nagao[1], Tetsuro Kobayashi[1], Kazuyo Moro[2], Manabu Ohyama[1], Takeya Adachi[1], Daniela Y Kitashima[1], Satoshi Ueha[3], Keisuke Horiuchi[4,5], Hideaki Tanizaki[6], Kenji Kabashima[6], Akiharu Kubo[1,5], Young-hun Cho[7], Björn E Clausen[8], Kouji Matsushima[3], Makoto Suematsu[9,10], Glaucia C Furtado[11], Sergio A Lira[11], Joshua M Farber[12], Mark C Udey[7] & Masayuki Amagai[1]

Langerhans cells (LCs) are epidermal dendritic cells with incompletely understood origins that associate with hair follicles for unknown reasons. Here we show that in response to external stress, mouse hair follicles recruited Gr-1^{hi} monocyte-derived precursors of LCs whose epidermal entry was dependent on the chemokine receptors CCR2 and CCR6, whereas the chemokine receptor CCR8 inhibited the recruitment of LCs. Distinct hair-follicle regions had differences in their expression of ligands for CCR2 and CCR6. The isthmus expressed the chemokine CCL2; the infundibulum expressed the chemokine CCL20; and keratinocytes in the bulge produced the chemokine CCL8, which is the ligand for CCR8. Thus, distinct hair-follicle keratinocyte subpopulations promoted or inhibited repopulation with LCs via differences in chemokine production, a feature also noted in humans. Pre-LCs failed to enter hairless skin in mice or humans, which establishes hair follicles as portals for LCs.

Hair represents a vital component of the skin, as it constitutes a physical barrier that protects mammals from external insults. Each individual hair follicle is equipped with anatomically distinct stem cell niches (the hair-follicle bulge), characterized by expression of the adhesion molecule CD34, integrin α_6 and keratin 15 (refs. 1–3), that facilitate the regeneration and maintenance of hair growth. Several studies have suggested that the hair follicle, particularly the bulge, represents an immune-privileged structure[4] that protects itself from undesirable inflammation via loss of major histocompatibility molecules or via the expression of CD200 (ref. 5), a cell-surface molecule reported to exert immunosuppressive effects[6].

Notably, hair follicles are targeted in several autoimmune and/or inflammatory diseases. The bulb is targeted in alopecia areata, which results in reversible hair loss, whereas the bulge is destroyed in lupus erythematosus and lichen planopilaris, which leads to irreversible hair loss[7]. Furthermore, hair follicles are densely populated by Langerhans cells (LCs), unique dendritic cells (DCs) of the epidermis characterized by radioresistance and longevity[8], simultaneous expression of the LC markers langerin and EpCAM (epithelial cell adhesion molecule)[9–11] and critical dependence on the cytokine TGF-β (transforming growth factor-β)[12–14]. LCs serve critical roles in host defense against pathogens on the skin surface by specifically promoting responses of the T_H17 subset of helper T cells against *Candida albicans*[15] and humoral responses of the T_H2 subset of helper T cells against bacterial antigen in mice immunized with the antigen via a gene gun[11], as well as against *Staphylococcus aureus*–derived toxin[16]. The importance of the association of LCs with hair follicles is unknown, and the specific mechanisms by which LCs associate with hair follicles remain unexplored.

LCs are reported to self-renew in skin at steady state[8] and to arise from a subset of monocytes identified by high expression of the monocyte marker Gr-1 (Ly6G) during inflammation elicited by irradiation with ultraviolet C waves[17]. It has also been reported that during development, LCs arise from lineages that express the chemokine receptor CX3CR1 (ref. 18). The relative contributions of monocytes and CX3CR1-expressing lineages as sources of LCs in adult mice are unknown. Furthermore, the route(s) and mechanisms by which precursors of LCs populate the epidermis remain unclear.

Many chemokine–chemokine receptor pairs coordinate the migration of DCs[19]. Skin DCs express chemokine receptors, and of those, CCR7 (refs. 20,21) and CXCR4 (ref. 22) are reported to be involved in the migration of LCs to the lymph nodes. The requirements for

[1]Department of Dermatology, Keio University School of Medicine, Tokyo, Japan. [2]Laboratory for Immune Cell System, RIKEN Research Center for Allergy and Immunology, Yokohama, Japan. [3]Department of Preventive Medicine, University of Tokyo, Tokyo, Japan. [4]Department of Orthopedics, Keio University School of Medicine, Tokyo, Japan. [5]Center for Integrated Medical Research, Keio University School of Medicine, Tokyo, Japan. [6]Department of Dermatology, Kyoto University Faculty of Medicine, Kyoto, Japan. [7]Dermatology Branch, Center for Cancer Research, National Cancer Institute, US National Institutes of Health, Bethesda, Maryland, USA. [8]Department of Immunology, Erasmus University Medical Center, Rotterdam, The Netherlands. [9]Department of Biochemistry, Keio University School of Medicine, Tokyo, Japan. [10]Japan Science and Technology Agency, Exploratory Research for Advanced Technology, Suematsu Gas Biology Project, Tokyo, Japan. [11]Immunology Institute, Mount Sinai School of Medicine, New York, New York, USA. [12]Laboratory of Molecular Immunology, National Institute of Allergy and Infectious Diseases, US National Institutes of Health, Bethesda, Maryland, USA. Correspondence should be addressed to K.N. (nagaok@med.keio.ac.jp).

Received 1 February; accepted 30 May; published online 24 June 2012; doi:10.1038/ni.2353

chemokine–chemokine receptor pairs by LCs during epidermal repopulation are incompletely characterized, in part because of the lack of knowledge about the origin of LCs and the route(s) of repopulation. However, the chemokine receptors CCR2 and CCR6 are known to enable monocyte-derived precursor cells to appear in epidermis as fully developed LCs[8,23]. In this report, we demonstrate that lysozyme M (LysM)-expressing myeloid cells gave rise to LCs after the application of mechanical or inflammatory stimuli to the skin and that these cells were induced to enter the epidermis by keratinocyte subsets in the hair follicle with distinct chemokine-expression profiles. Precursors of LCs did not efficiently populate the epidermis if they did not express the appropriate chemokine receptors or if the hair follicles were absent. Thus, our results demonstrate a previously unknown contribution of hair follicles to the entry of DCs into sites of limited or minor tissue perturbation.

RESULTS

Langerin-negative DCs populate epidermis depleted of LCs

To monitor repopulation by LCs, we studied mice with sequence encoding the diphtheria toxin receptor (DTR) inserted into the gene encoding langerin (Langerin-DTR mice), which allows inducible ablation of LCs by treatment with diphtheria toxin (DT)[24]. Langerin-DTR mice underwent rapid depletion of epidermal LCs, which express langerin, after intraperitoneal administration of DT; the LCs reappeared in clusters over a period of weeks to months in the absence of perturbation[11,24] (**Fig. 1a**). The repopulating LCs coexpressed the LC markers langerin and EpCAM[11]. To ensure that those clusters of LCs did not reflect incomplete depletion, we generated bone marrow chimeras by reconstituting lethally irradiated Langerin-DTR (CD45.1$^+$) mice with bone marrow from wild-type (CD45.2$^+$) mice. At 3–8 weeks after reconstitution, all hematopoietic cells in the recipient mice were of donor origin, except for radioresistant epidermal LCs, which remained mainly of host origin[8] (data not shown). Depleting the mice of LCs by treatment with DT at this point allowed us to monitor the appearance of LCs of donor origin. Langerin-expressing LCs repopulated the epidermis in clusters. However, staining for major histocompatibility complex (MHC) class II also identified langerin-negative (Lang$^-$) cells in the epidermis (**Fig. 1b**). These Lang$^-$ cells were present either as single cells or clusters and could be readily distinguished by their size and highly dendritic morphology (**Fig. 1b**).

To determine if MHC class II–positive (MHCII$^+$), Lang$^-$ cells entered the epidermis only after mice were depleted of LCs, we analyzed suspensions of epidermal cells from wild-type mice or from lethally irradiated Langerin-DTR mice that had been reconstituted with congenic bone marrow and then treated intraperitoneally with DT (or PBS as a control) 14 d before analysis. Although most MHCII$^+$ cells in wild-type mice expressed langerin, we observed some MHCII$^+$Lang$^-$ cells in control Langerin-DTR bone marrow chimeras that received PBS (**Fig. 1c**). DT-treated Langerin-DTR bone marrow chimeras had three- to fivefold more donor-derived MHCII$^+$Lang$^-$ cells than did their PBS-treated counterparts (**Fig. 1c**), which demonstrated that depleting mice of LCs facilitated epidermal infiltration or population expansion by MHCII$^+$Lang$^-$EpCAM$^-$ cells.

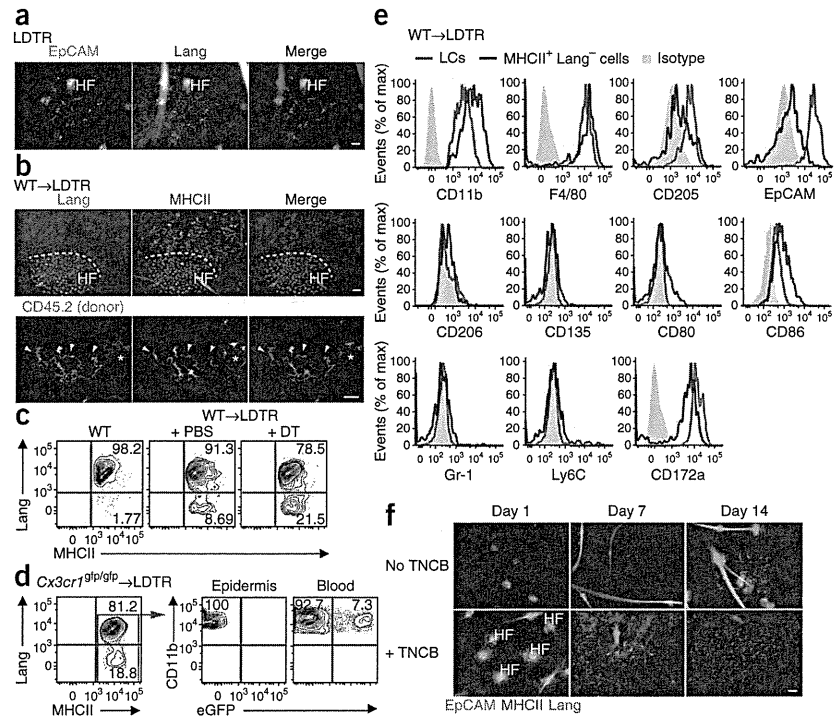

Figure 1 MHCII$^+$Lang$^-$ cells of myeloid phenotype infiltrate epidermis depleted of LCs. (**a**) Immunofluorescence microscopy of epidermal sheets from Langerin-DTR (LDTR) mice 14 d after depletion of LCs via treatment with DT, stained to detect EpCAM and langerin. HF, hair follicle. Scale bar, 20 μm. (**b**) Microscopy of ear epidermis from Langerin-DTR (CD45.1$^+$) mice reconstituted with congenic (CD45.2$^+$) wild-type (WT) donor bone marrow (WT→LDTR) 2 weeks after DT-mediated depletion of host-derived LCs, stained to detect MHC class II and langerin. Arrowheads indicate donor-derived MHCII$^+$Lang$^-$ cells; asterisks indicate conventional LCs. Scale bars, 50 μm (top) or 20 μm (bottom). (**c**) Flow cytometry of epidermal cells from wild-type (CD45.2$^+$) mice (WT) and from Langerin-DTR (CD45.1$^+$) mice reconstituted with wild-type bone marrow (WT→LDTR) and treated with PBS or DT 3 weeks later, followed by analysis 2 weeks later. Numbers in quadrants indicate percent cells in each throughout. (**d**) Flow cytometry of epidermal cells and peripheral blood from Langerin-DTR mice ($n = 6$) reconstituted with *Cx3cr1*$^{gfp/gfp}$ (CD45.2$^+$) bone marrow (*Cx3cr1*$^{gfp/gfp}$→LDTR) and treated with DT, followed by analysis 2 weeks later, in parallel with **c**. Cells were gated on CD45.2$^+$MHCII$^+$CD11b$^+$ cells in **c**,**d**. (**e**) Surface phenotype of LCs and MHCII$^+$Lang$^-$ cells from the epidermis of Langerin-DTR mice ($n = 3$) reconstituted with wild-type (CD45.2$^+$) bone marrow, assessed by flow cytometry with gating on CD45.2$^+$MHCII$^+$ cells that were either Lang$^+$EpCAM$^+$ (LCs) or Lang$^-$EpCAM$^-$ for analysis of CD11b (top left), or on CD45.2$^+$MHCII$^+$CD11b$^+$ cells (all other plots). Isotype, isotype-matched control antibody. (**f**) Microscopy of ear epidermal sheets from Langerin-DTR mice ($n = 3$) treated with DT on day −1 and painted with TNCB on day 0, collected on days 7 and 14 and stained for EpCAM, MHC class II and langerin. Scale bar (**f**), 20 μm. Data are from one experiment representative of five independent experiments with three to five mice per group in each (**a**–**c**) or are representative of two (**d**,**e**) or three (**f**) independent experiments.

To determine if the MHCII$^+$Lang$^-$EpCAM$^-$ cells were related to the CX3CR1$^+$ precursors of LCs that seed the epidermis during embryonic development[18], we transferred bone marrow from wild-type and *Cx3Cr1*$^{gfp/gfp}$ mice (in which sequence encoding enhanced green fluorescent protein (eGFP) is knocked into the gene encoding CX3CR1 (*Cx3Cr1*) to inactivate *Cx3Cr1*)[25] into lethally irradiated Langerin-DTR mice, then treated the mice with DT to deplete them of LCs at 3 weeks after transplantation of bone marrow. *Cx3Cr1*$^{gfp/gfp}$ LCs and MHCII$^+$Lang$^-$ cells populated the epidermis with efficiency similar to that achieved by wild-type cells (**Fig. 1c,d**), which indicated that CX3CR1 was not required for repopulation by LCs. Furthermore, although we detected eGFP expression in leukocytes in the blood, we did not detect it in LCs or MHCII$^+$Lang$^-$ cells that repopulated the epidermis (**Fig. 1d**), which suggested that the LCs in this repopulation setting were distinct from the CX3CR1-expressing lineage.

We used flow cytometry to better characterize the epidermis-repopulating MHCII$^+$Lang$^-$ cells. MHCII$^+$Lang$^-$ cells had higher CD11b expression and lower CD205 expression than did LCs, but had F4/80 expression similar to that of LCs, and expressed little if any EpCAM. MHCII$^+$Lang$^-$ cells also had slightly higher expression of CD80 and CD86 than LCs had, whereas their CD172a expression was slightly lower than that on LCs (**Fig. 1e**). We did not detect CD206 or CD135 on either cell type. We also did not detect expression of Gr-1 or Ly6C by these cells (**Fig. 1e**). Together these data indicated that MHCII$^+$ cells of donor bone marrow origin with a myeloid phenotype repopulated epidermis that had been depleted of LCs and that they seemed to be distinct from both the CX3CR1$^+$ precursors of LCs and Gr-1^{hi} precursors of LCs reported before[17,18].

Rapid repopulation by LCs during inflammation

The detection of low expression of langerin in some MHCII$^+$ cells with highly dendritic morphology in the bone marrow chimeras suggested that MHCII$^+$Lang$^-$ cells might differentiate into LCs (data not shown). To explore the possibility that differentiation into LCs was enhanced by inflammation, we monitored repopulation by LCs in Langerin-DTR mice depleted of LCs that also received one application of the hapten TNCB to the ear skin 1 d after being depleted of LCs. In contrast to the slow repopulation by LCs observed after treatment with DT in ears not treated with TNCB, MHCII$^+$Lang$^-$EpCAM$^-$ cells infiltrated TNCB-treated epidermis on day 1 after treatment (**Fig. 1f** and **Supplementary Fig. 1**), acquired various amounts of expression of langerin and EpCAM by day 7, and almost completely reconstituted the epidermis with fully differentiated LCs by day 14 (**Fig. 1f**). These findings suggested that MHCII$^+$Lang$^-$EpCAM$^-$ cells were the immediate precursors of true LCs and that differentiation into LCs could be enhanced by inflammation.

Generation of LCs by LysM-expressing MHCII$^+$ cells

We sought to determine the origin of the MHCII$^+$Lang$^-$EpCAM$^-$ potential precursors of LCs. To investigate if these were derived from monomyeloid precursors[26], as indicated by their myeloid phenotype, we mapped the fate of LysM-expressing cells by crossing mice expressing Cre recombinase driven by the gene expressing LysM (LysM-Cre mice), which allows myeloid cell–specific deletion of *lox*P-flanked genes by Cre[27], to mice with transgenic expression of *lox*P-flanked sequence encoding chloramphenicol acetyltransferase (CAT) and eGFP driven by the CAG promoter (chicken β-actin promoter with cytomegalovirus enhancers; CAG-CAT-eGFP mice)[28]. In the resulting

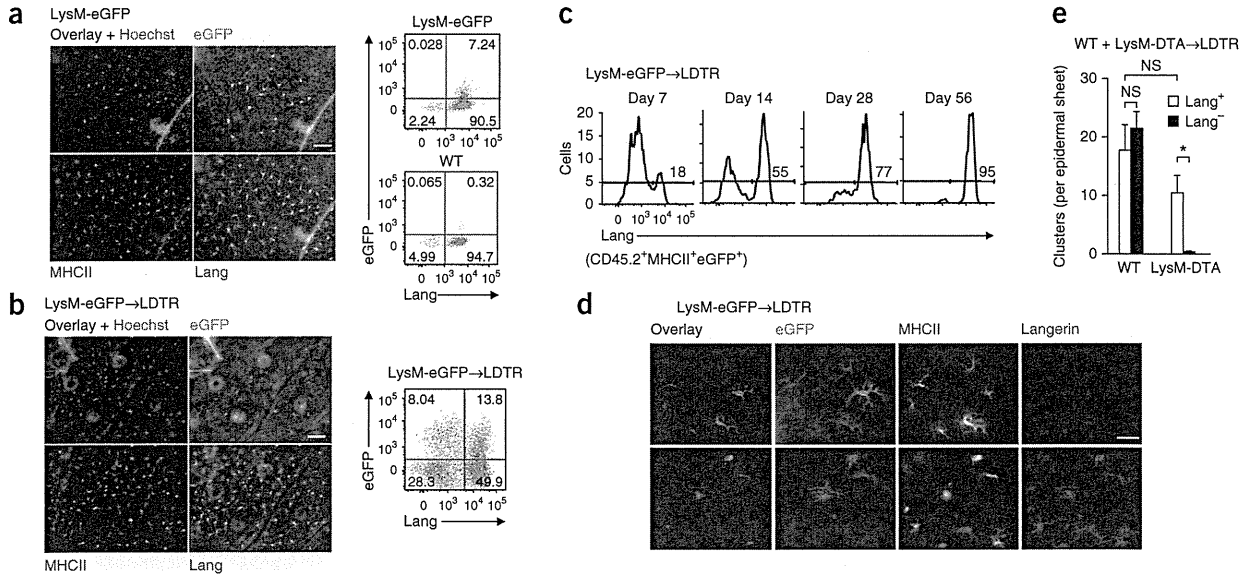

Figure 2 LysM-expressing precursors give rise to a subset of LCs. (**a**,**b**) Immunofluorescence microscopy (left) of epidermal sheets from LysM-eGFP mice (**a**) or from Langerin-DTR (CD45.1$^+$) mice reconstituted with LysM-eGFP (CD45.2$^+$) bone marrow (LysM-eGFP→LDTR), treated with DT 3 weeks later, then treated with TNCB and analyzed 2 weeks later (**b**). Scale bars, 50 μm. Right, flow cytometry of epidermal cell suspensions assessing the expression of eGFP and langerin on cells gated for CD45.2, MHCII and CD11b. (**c**) Langerin expression by LysM^{fm+} cells in the epidermis of Langerin-DTR mice reconstituted with LysM-eGFP bone marrow and treated with TNCB, assessed 7, 14, 28 and 56 d later. (**d**) Microscopy of epidermal sheets from Langerin-DTR mice reconstituted with CD115$^+$Gr-1^{hi} LysM-eGFP bone marrow cells, then treated with DT 3 weeks later and TNCB on the next day, followed by analysis 14 d later by staining for eGFP, MHC class II and langerin. Scale bar, 25 μm. (**e**) Quantification of clusters of LCs (MHCII$^+$Lang$^+$) or pre-LCs (MHCII$^+$Lang$^-$) of each bone marrow origin in Langerin-DTR mice reconstituted with a mixture of equal numbers of wild-type (CD45.1$^+$) and LysM-DTA (CD45.2$^+$) bone marrow cells (WT + LysM-DTA→LDTR), then treated with DT and analyzed 2 weeks later. NS, not significant; $^*P = 0.0021$ (unpaired two-tailed Student's *t*-test). Data are from one experiment representative of three (**a**,**b**) or two (**c**–**e**) independent experiments with three (**a**–**c**,**e**) or two (**d**) mice per group in each (mean and s.e.m. in **e**).

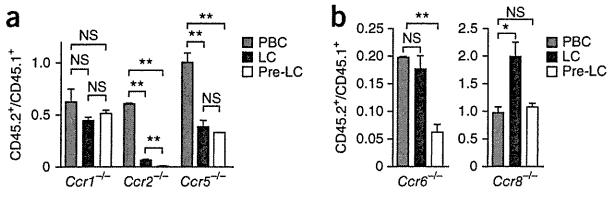

Figure 3 Dependence of LCs and pre-LCs on chemokine receptors. Flow cytometry of peripheral blood cells (PBC) and epidermal cells (LC and pre-LC) from Langerin-DTR mice reconstituted with a mixture of equal numbers of wild-type ($CD45.1^+$) bone marrow cells and $CD45.2^+$ bone marrow cells deficient in CCR1, CCR2 or CCR5 (**a**) or CCR6 or CCR8 (**b**), followed 3 weeks later by DT-mediated depletion of recipient mice of host LCs and analysis of the ratio of $CD45.2^+$ cells to $CD45.1^+$ cells among $MHCII^{hi}CD11b^{hi}$ cells ($CD45.2^+/CD45.1^+$) 2 weeks later. $*P = 0.0172$ and $**P < 0.006$ (unpaired two-tailed Student's *t*-test). Data are from one experiment representative of two independent experiments with three to five mice per group in each (mean and s.e.m.).

LysM-eGFP offspring, the expression of eGFP marked cells that had previously expressed LysM (called '$LysM^{fm+}$ cells' here). We detected scattered clusters of $LysM^{fm+}$ ($MHCII^+Lang^+$) LCs in the unperturbed epidermis of LysM-eGFP mice by immunofluorescence microscopy. Flow cytometry showed that up to 10% of LCs in adult mice were derived from LysM-expressing precursor cells (**Fig. 2a**). To verify that $LysM^{fm+}$ cells originated in bone marrow, we transferred bone marrow from LysM-eGFP ($CD45.2^+$) mice into Langerin-DTR ($CD45.1^+$) mice, then depleted the mice of host LCs by treatment with DT and then treated the mice topically with TNCB 3 weeks later. Staining of epidermal sheets 2 weeks after that treatment with TNCB routinely demonstrated the presence of donor $CD45.2^+LysM^{fm+}$ LCs. Consistent with that, 20–30% of $MHCII^+CD45.2^+$ epidermal cell suspensions were $LysM^{fm+}$, and up to 35% of $Lang^+$ LCs were $LysM^{fm+}$ (**Fig. 2b**). Only 50% of the epidermal LCs in CAG-eGFP mice expressed eGFP (data not shown), consistent with published observations that strong viral promoters, such as the CAG promoter used here, can undergo silencing[29]. Therefore, the number of $LysM^{fm+}$ LCs and/or precursors of LCs in these experiments might be underestimated.

We next evaluated the time course of repopulation by and differentiation of $LysM^{fm+}$ LCs in bone marrow chimeras. At day 7 after TNCB treatment, suspensions of epidermal cells from dorsal trunk skin contained $LysM^{fm+}MHCII^+$ cells, only a small fraction of which expressed langerin. At day 14, over 50% of $LysM^{fm+}$ cells expressed langerin, and by days 28 and 56, most $LysM^{fm+}$ cells persisted and had acquired langerin expression (**Fig. 2c**). These data demonstrated that a subpopulation of LCs in unperturbed skin, as well as in chimeras, arose from a LysM-expressing lineage. We called the $LysM^{fm+}MHCII^+Lang^-$ cells that infiltrated the epidermis after bone-marrow transfer or inflammation 'pre-LCs'.

To determine whether the pre-LCs were derived from $Gr\text{-}1^{hi}$ monocyte precursors[17], we reconstituted irradiated Langerin-DTR mice with $CD115^+Gr\text{-}1^{hi}$ LysM-eGFP bone marrow, then depleted the mice of host LCs through treatment with DT and induced pre-LCs by topical application of TNCB. Two weeks later, we found eGFP-expressing pre-LCs and LCs in the ear epidermis (**Fig. 2d**), which demonstrated that $CD115^+Gr\text{-}1^{hi}$ cells in the bone marrow gave rise to pre-LCs, which further differentiated into LCs. $MHCII^+CD11b^{hi}$ or $MHCII^+CD11b^{lo}$ DCs in the skin, which represented dermal DCs that included $Lang^-$ and $Lang^+$ dermal DCs, did not express any eGFP (data not shown).

To confirm those findings, we crossed LysM-Cre mice to mice that express the gene encoding diphtheria toxin A (DTA) from the ubiquitous *Rosa26* locus. In the resulting LysM-DTA offspring, cells that expressed LysM simultaneously expressed DTA and underwent cell death, which led to constitutive depletion of cells of the LysM-expressing lineage. We reconstituted lethally irradiated Langerin-DTR mice with a mixture of equal numbers of LysM-DTA ($CD45.2^+$) bone marrow cells and wild-type ($CD45.1^+$) bone marrow cells, then depleted the mice of host LCs through treatment with DT 3 weeks later. In contrast to wild-type bone marrow, which gave rise to both true LCs and pre-LCs 2 weeks after mice were depleted of LCs, LysM-DTA bone marrow did not produce pre-LCs (**Fig. 2e**). The absence of pre-LCs reproducibly led to fewer fully developed LCs, but mice never underwent complete depletion of LCs, consistent with the observation that most LCs in LysM-eGFP mice did not express eGFP (**Fig. 2a,b**). Thus, monomyeloid pre-LCs gave rise to a subpopulation of LCs during steady state or after perturbation in adult mice but did not represent

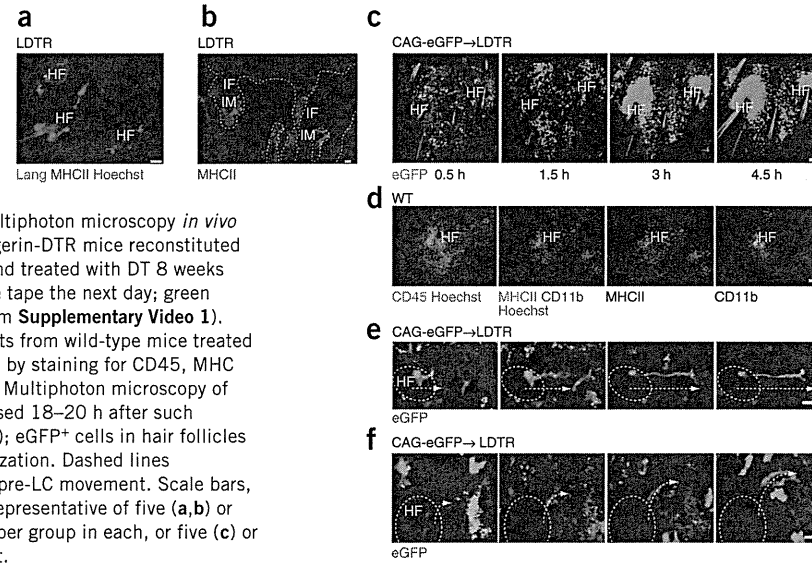

Figure 4 Pre-LCs repopulate the epidermis via hair follicles. (**a**) Immunofluorescence microscopy of epidermal sheets from Langerin-DTR mice depleted of LCs and then treated with TNCB, stained 1 d later for langerin and MHC class II. (**b**) Immunofluorescence microscopy of lip sections from Langerin-DTR mice treated with DT, stained 2 weeks later for MHC class II. Dashed lines delineate hair follicles. IF, infundibulum; IM, isthmus. (**c**) Multiphoton microscopy *in vivo* of the infiltration of leukocytes into the ears of Langerin-DTR mice reconstituted with CAG-eGFP bone marrow (CAG-eGFP→LDTR) and treated with DT 8 weeks later, followed by stripping of the ears with adhesive tape the next day; green cells represent donor-derived leukocytes (images from **Supplementary Video 1**). (**d**) Immunofluorescence microscopy of dermal sheets from wild-type mice treated by stripping of the ears with adhesive tape, followed by staining for CD45, MHC class II and CD11b (below images) 4.5 h later. (**e**,**f**) Multiphoton microscopy of an ear from a different mouse treated as in **c**, assessed 18–20 h after such tape stripping (images from **Supplementary Video 2**); $eGFP^+$ cells in hair follicles have been pseudocolored orange to facilitate visualization. Dashed lines delineate hair follicles; arrows indicate direction of pre-LC movement. Scale bars, 20 μm (**a**,**b**), 50 μm (**c**,**d**) or 10 μm (**e**,**f**). Data are representative of five (**a**,**b**) or three (**d**) independent experiments with three mice per group in each, or five (**c**) or six (**e**,**f**) experiments with one mouse per experiment.

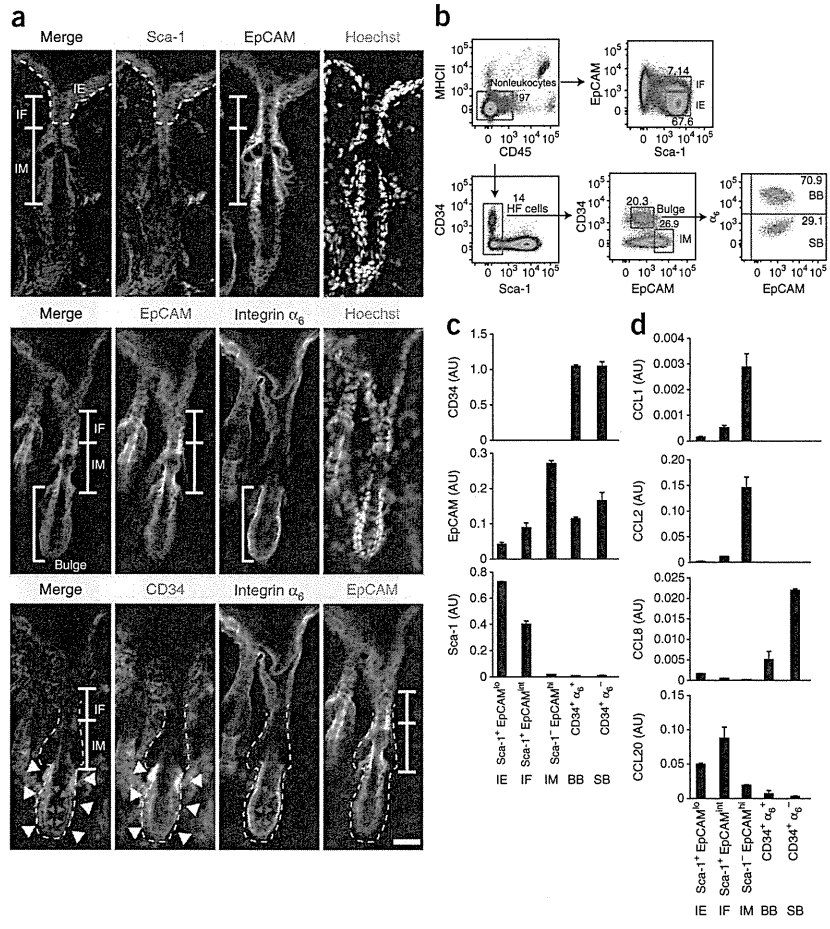

Figure 5 Hair-follicle keratinocyte subsets are the main source of chemokines that regulate the entry of LCs. (**a**) Immunofluorescence microscopy of frozen sections of mouse skin stained for various molecules (above images) to delineate the interfollicular epidermis (IE), infundibulum (IF), isthmus (IM), basal bulge (BB) and suprabasal bulge (SB) in hair follicles in telogen. Arrowheads (white) and arrows (red) indicate basal bulge and suprabasal bulge, respectively. Scale bar, 20 μm. (**b**) Flow cytometry of epidermal keratinocytes from interfollicular epidermis and hair follicles to sort into five subsets (as in **a**) by their expression of surface markers. Numbers adjacent to or in outlined areas indicate percent cells in each. (**c**) Real-time PCR analysis of the expression of CD34, EpCAM and Sca-1 mRNA in sorted hair-follicle keratinocyte subsets (below horizontal axis), presented (in arbitrary units (AU)) relative to the expression of GAPDH mRNA (encoding glyceraldehyde phosphate dehydrogenase). (**d**) Real-time PCR analysis of the expression of CCL1, CCL2, CCL8 and CCL20 mRNA in sorted hair-follicle keratinocyte subsets (presented as in **c**). Data are from one experiment representative of three (**a**,**b**) or two (**c**,**d**) independent experiments (pooled from three mice per experiment in **b**; mean and s.d. in **c**,**d**).

the sole source of LCs. LCs that were independent of monomyeloid pre-LCs also arose from the bone marrow, but their exact origin(s) remain(s) to be identified. Together these data suggested that several pathways support LC development and that the relative importance of the different pathways may vary over the life of a mouse and is influenced by the presence or absence of environmental perturbation (such as ultraviolet irradiation, infection and allergic or physical insults).

Pre-LCs require chemokine receptors for entry into the epidermis

To evaluate chemokine-receptor use by LCs and pre-LCs, we reconstituted Langerin-DTR mice with a mixture of an equal number of bone marrow cells from CD45.2$^+$ mice deficient in CCR1, CCR2, CCR5, CCR6 or CCR8 and from wild-type (CD45.1$^+$) mice, then depleted the mice of host LCs through treatment with DT 3 weeks later. Because of the potential effect of chemokine-receptor deficiency on the migration of cells from the bone marrow into the circulation, we compared the ratio of CD45.2$^+$ (chemokine receptor–deficient) cells to CD45.1$^+$ (wild-type) cells in blood and epidermis to determine which chemokine receptors were required for the entry of pre-LCs into the epidermis.

A lower ratio of CD45.2$^+$ cells to CD45.1$^+$ cells among MHCII^{hi} CD11b^{hi} cells (a phenotype similar to that of LCs and pre-LCs) in the peripheral blood showed that CCR1, CCR2 and CCR6 were required for entry into the circulation. Deficiency in CCR5 or CCR8 did not affect this ratio (**Fig. 3**). Whereas the lack of CCR1 had no effect on the entry of LCs or pre-LCs into the epidermis, deficiency in CCR2 or CCR5 had a substantial effect on both LCs and pre-LCs at this stage, with CCR2 deficiency having a stronger effect than CCR5 deficiency had (**Fig. 3a**). CCR6 deficiency affected mainly pre-LCs, which demonstrated that chemokine receptors were used differently during repopulation of the epidermis by LCs and pre-LCs. Fully developed LCs derived from CCR6-deficient bone marrow were not significantly affected by the much lower abundance of pre-LCs (**Fig. 3b**), which suggested a steady-state source of LCs that was independent of the LysM-expressing lineage. CCR8 deficiency resulted in enhanced repopulation of epidermis by LCs but not by pre-LCs (**Fig. 3b**), which indicated that the ligand(s) for CCR8 negatively regulated the repopulation of the epidermis by LCs but not by pre-LCs. These results demonstrated that LCs and pre-LCs used chemokine receptors differently during repopulation of the epidermis.

Entry of pre-LCs into the epidermis via the hair follicles

We next sought to determine the route by which pre-LCs infiltrated the epidermis. We regularly observed pre-LCs in close association with the hair follicles in epidermal sheets during early TNCB-induced repopulation in DT-treated Langerin-DTR mice (**Figs. 1f** and **4a**). MHCII$^+$ cells (presumably pre-LCs) localized to follicular structures of hair follicles, particularly the infundibulum and isthmus, during repopulation (**Fig. 4b**).

Because the dynamics of cell infiltration cannot be assessed in fixed *ex vivo* tissues, we assessed leukocytic infiltration in skin by intravital multiphoton microscopy. We reconstituted lethally irradiated Langerin-DTR mice with bone marrow cells from CAG-eGFP mice, in which expression of eGFP is driven by the ubiquitous CAG promoter, and depleted the mice of host LCs via treatment with DT. We observed infiltration of the ear skin by eGFP-expressing cells *in vivo* after gentle stripping of the skin with adhesive tape (data not shown), a procedure

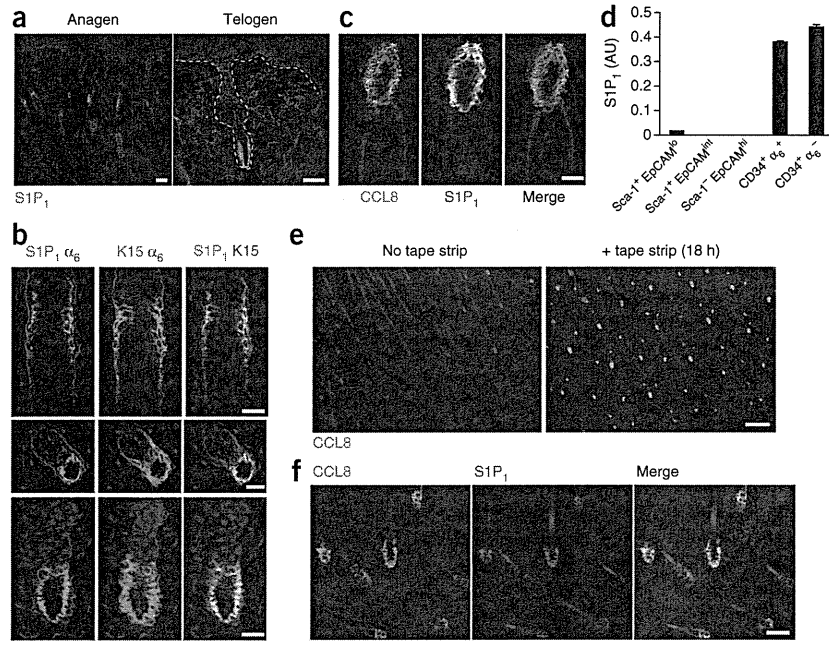

Figure 6 $S1P_1$ expression identifies CCL8-producing suprabasal hair-follicle bulge cells. (**a**) Confocal microscopy of hair follicles in anagen and telogen in frozen sections of mouse skin stained for $S1P_1$. (**b**) Microscopy of vertical frozen skin sections of a hair follicle in anagen (top), a cross-section of a hair follicle in early anagen (middle) and a vertical section of a hair follicle in telogen (bottom), stained for $S1P_1$, integrin α_6 or keratin 15 (K15). (**c**) Microscopy of a cross-section of a hair follicle, stained for CCL8 and $S1P_1$. (**d**) Real-time PCR analysis of the expression of $S1P_1$ mRNA in sorted hair-follicle keratinocyte subsets (from **Fig. 5c,d**; presented as in **Fig. 5c**). (**e**) Immunofluorescence microscopy of epidermal ear sheets from mice given no tape stripping (left) or treated to tape stripping 18 h before collection (right), stained for CCL8. (**f**) Confocal microscopy of epidermal sheets from mouse ears treated to tape stripping 18 h before collection, stained for CCL8 and $S1P_1$. Scale bars, 100 μm (**a**, left), 50 μm (**a**, right), 20 μm (**b**,**c**,**f**) or 100 μm (**e**). Data are representative of three to five independent experiments with three mice per group in each (mean and s.d. in **d**).

removes approximately three fourths of the cornified layers but leaves most hairs intact. We found that $eGFP^+$ leukocytes appeared in the dermis within 0.5 h of such tape stripping, and these cells accumulated near the follicular structures (**Fig. 4c** and **Supplementary Video 1**). Leukocytes that accumulated near the hair follicle were mainly $MHCII^+$ and $CD11b^+$ and probably represented dermal DCs and some pre-LCs (**Fig. 4d**). At approximately 18–20 h after the tape-stripping procedure, $eGFP^+$ cells with dendritic morphology (pre-LCs) appeared in hair follicles and extended dendrites or crawled into the interfollicular epidermis (**Fig. 4e,f** and **Supplementary Video 2**). These observations suggested that after mechanical stress, leukocytes (particularly myeloid DCs) were recruited to the skin via hair follicles and that a small fraction of these cells, representing pre-LCs, were guided into the epidermis through these structures.

Differences in the expression of chemokines by the hair follicle

We next determined if hair follicles (and within those, different keratinocyte subsets) produced ligands for the chemokine receptors that were necessary for efficient infiltration of the epidermis by LCs and pre-LCs. To find cell-surface markers distinctively expressed by different follicular keratinocyte subsets, we did immunofluorescence staining for the hematopoietic stem-cell marker Sca-1, EpCAM, integrin α_6 and CD34. Sca-1 expression was limited to the interfolliclar epidermis and infundibulum[30] (**Fig. 5a**). EpCAM, which is expressed specifically by LCs among skin DCs and in the hair follicles during embryonic development[31], was expressed throughout the whole epidermis in adult mice and also had high expression in the infundibulum and isthmus, especially the latter (**Fig. 5a**). CD34 expression was limited to the bulge area, an area that contains hair follicle and melanocyte stem cells[1,32], and integrin α_6 expression was limited to the basal layers (**Fig. 5a**). On the basis of those patterns of expression, we sorted keratinocyte subsets from the interfollicular epidermis, infundibulum, isthmus, basal bulge and suprabasal bulge (**Fig. 5b**). Real-time PCR analysis of cDNA obtained from sorted keratinocyte subsets confirmed that the expression of CD34 mRNA was limited to the bulge (basal and suprabasal layers), whereas expression of EpCAM mRNA was present in all epidermal components but was highest in the isthmus (**Fig. 5c**). We detected Sca-1 mRNA in the interfollicular epidermis and infundibulum (**Fig. 5a,c**).

Analysis of the expression of mRNA for various chemokines in sorted hair-follicle keratinocyte subsets showed that distinct compartments in hair follicles had different expression of the chemokines of interest. CCL20 (the ligand for CCR6) was expressed mainly by infundibular cells (**Fig. 5d**). CCL1 (a ligand for CCR8) and CCL2 (the ligand for CCR2) were expressed exclusively in the isthmus (**Fig. 5d**). We did not detect CCL3, CCL4 or CCL5, which are ligands for CCR5, in any epidermal compartment, which suggested that CCR5 functions outside the epidermal compartment during repopulation with LCs and pre-LCs. Although we did not detect any of these chemokine mRNAs in $CD34^+$, integrin α_6–positive basal bulge cells, we found expression of mRNA for CCL8 (a ligand for CCR8) exclusively in $CD34^+$, integrin α_6–negative suprabasal bulge cells (**Fig. 5d**). These data demonstrated that in the epidermal component, hair-follicle keratinocytes represented a chief source of chemokines able to promote or inhibit the recruitment of LCs and pre-LCs during epidermal repopulation (**Supplementary Fig. 2**).

Suprabasal bulge cells express CCL8 in response to stress

Next we attempted to visualize the chemokines of interest *in situ* in skin. We detected expression of $S1P_1$, a molecule involved in the trafficking of lymphocytes[33,34] and osteoclasts[35], as well as in angiogenesis[36], in a subset of cells in the bulge of hair follicles in anagen (the growing phase) or telogen (the resting phase; **Fig. 6a**), rather than in leukocytes. These cells were bulge keratinocytes, as defined by expression of keratin 15 and CD34 (**Fig. 6b** and **Supplementary Fig. 3**), and were distinct from the pool of hair-follicle bulge stem cells by the absence of integrin α_6 (**Fig. 6b**). $S1P_1^+$ bulge cells represented a sharply demarcated cluster of cells that resided strictly above the basal layer (**Fig. 6b**).

We were unable to visualize CCL1, CCL2 or CCL20 by immunofluorescence microscopy, possibly because of their soluble nature, but we detected CCL8 in some hair follicles (**Fig. 6c**). Consistent with the mRNA data (**Fig. 5d**), CCL8 localized exclusively to $S1P_1^+$

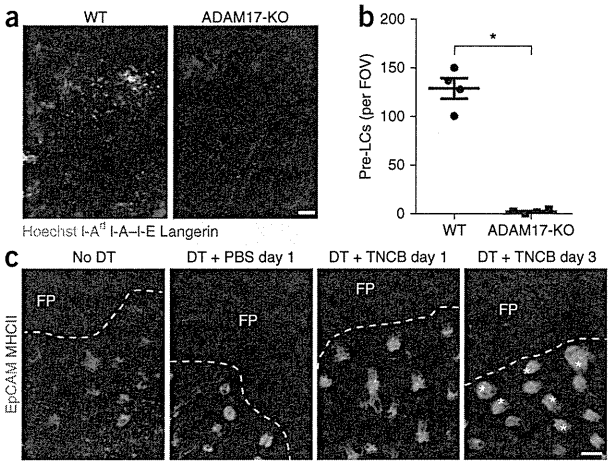

Figure 7 Pre-LCs fail to populate hairless epidermis. (**a**) Immunofluorescence microscopy of epidermal sheets from nude mice given simultaneous grafting of wild-type skin (WT) and *Adam17*$^{fl/fl}$Sox9-Cre skin (ADAM17-KO) onto opposite flanks, followed 2 months later by topical application of mometasone for 2 d (for depletion of LCs from skin grafts) and then treatment with TNCB (for induction of repopulation with pre-LCs) and staining for host-derived pre-LCs (I-A–I-E positive, I-A^d positive, langerin negative) 2 weeks later. Scale bar, 100 μm. (**b**) Quantification of pre-LCs in epidermal sheets in **a** at a magnification of ×200. FOV, field of view. Each symbol represents an individual mouse; small horizontal lines indicate the mean (and s.e.m.). *$P < 0.0001$ (unpaired two-tailed Student's *t*-test). (**c**) Immunofluorescence microscopy of footpad epidermal sheets from Langerin-DTR mice left untreated (No DT), or treated with DT on day −1, followed by painting of PBS (DT + PBS) or TNCB (DT + TNCB) onto the footpad (FP) and the surrounding hair-bearing skin on day 0 and staining for EpCAM and MHC class II on day +1 or +3. Dashed lines delineate the border between the footpad and hair-bearing epidermis; asterisks (far right) indicate hair follicles with infiltration by pre-LCs. Scale bar, 200 μm. Data are from one experiment representative of two independent experiments with two mice per group in each.

suprabasal bulge cells. Analysis of $S1P_1$ mRNA in sorted hair-follicle keratinocytes confirmed its expression in CD34$^+$ suprabasal keratinocytes as well as in basal bulge keratinocytes (**Fig. 6d**), which indicated that the expression of $S1P_1$ mRNA transcripts began in the basal layer but expression of $S1P_1$ protein was limited to suprabasal cells.

We observed uniform and substantial upregulation of CCL8 by $S1P_1^+$ hair follicle cells after the tape-stripping procedure (**Fig. 6e,f**). This indicated that this chemokine was induced in response to mechanical stress in skin. These results suggested that CCL8 may be produced in response to injury to protect the bulge area by preventing excessive influx of LCs.

Pre-LCs fail to repopulate epidermis in hairless skin in mice

Next we assessed the involvement of hair follicles in the recruitment of pre-LCs into the epidermis. Conditional depletion of the metalloprotease ADAM17 (TACE) from hair-follicle stem cells by deletion of *lox*P-flanked alleles encoding ADAM17 via Cre recombinase expressed under the control of the promoter of the gene encoding the transcription factor Sox9 (*Adam17*$^{fl/fl}$*Sox9*-Cre) results in permanent hair loss in mice. Sox9 is expressed in hair-follicle stem cells[37], and the permanent hair loss in *Adam17*$^{fl/fl}$*Sox9*-Cre mice resulted from failure of establishment of the hair-follicle bulge niche and maintenance of hair-follicle stem cells (data not shown). LC development in young *Adam17*$^{fl/fl}$*Sox9*-Cre mice was unaltered (data not shown). When grafted onto opposite flanks of nude mice, *Adam17*$^{fl/fl}$*Sox9*-Cre skin grafts were hairless, whereas the wild-type skin grafts grew hair (**Supplementary Fig. 4a,b**). After depleting mice of LCs, we evaluated infiltration by pre-LCs 1 week after treating the mice with TNCB. We detected host-derived pre-LCs (positive for the MHC class II molecule I-A^d, and langerin negative) in epidermal sheets from wild-type skin grafts, whereas the epidermis of *Adam17*$^{fl/fl}$*Sox9*-Cre skin grafts had considerably fewer pre-LCs (**Fig. 7a,b**).

We also evaluated repopulation of footpads, the center of which is hairless, by LCs in Langerin-DTR mice. LCs were sparsely present in footpads, in contrast to their abundant presence in hair-bearing epidermis (**Fig. 7c**). We depleted Langerin-DTR mice of LCs and treated them with TNCB and found that this induced the entry of pre-LCs into the epidermis via hair follicles; these LCs moved into hairless areas of the footpad by day 3 after treatment with TNCB (**Fig. 7c**). These observations established hair follicles as critical skin structures that guided the entry of pre-LCs into the epidermis and documented that hair follicle served as leukocyte-epithelial interfaces that actively regulated the trafficking of DCs in the skin in response to environmental stimuli.

Chemokine expression by human hair-follicle keratinocytes

To determine if our findings could be extended to humans, we studied chemokine expression in human scalp. The hair follicles of humans and mice have anatomical differences. Furthermore, whereas hair follicles are mainly in anagen in humans, they are mostly in telogen in mice. We therefore divided human scalp tissue into the following five parts on the basis of its anatomy, using a dissecting microscope: interfollicular epidermis, infundibulum, bulge, bulb and suprabulb[38]. We used real-time PCR to evaluate the expression of mRNA for chemokines involved during repopulation by LCs and pre-LCs in mice. Keratinocytes from human hair follicles showed distinct chemokine expression patterns. CCL2 and CCL20 were expressed in the infundibulum, as well as in the interfollicular epidermis (**Fig. 8a**). Whereas the bulge and the bulb did not have high expression of chemokine mRNA, the infundibulum and the suprabulb, especially the latter, expressed both CCL1 and CCL8 (**Fig. 8a**). We also evaluated the expression of chemokines that function as ligands for the chemokine receptor CXCR3, because CXCR3$^+$ T cells have been shown to invade the hair follicles in alopecia areata[39]. The chemokines CXCL4, CXCL9, CXCL10 and CXCL11 were all expressed mainly in the infundibulum and the suprabulb (**Fig. 8a**), an expression pattern nearly identical to that of CCL1 and CCL8. These results suggested that keratinocytes of human hair follicles produced distinct chemokines, with the infundibulum and the suprabulb representing the main sites of chemokine production in humans.

Lack of LCs in hairless human epidermis

Finally, we studied human skin from patients with alopecia. Alopecia areata and lichen planopilaris are characterized by lymphocytic infiltration of hair follicles and hair loss[7]. However, lymphocytic inflammation spares stem cell–containing hair-follicle bulge regions in alopecia areata, which results in reversible hair loss, whereas the bulge region is targeted in lichen planopilaris, which results in stem-cell destruction and permanent hair loss. We found that whereas LCs were present in the interfollicular epidermis of scalps from normal human subjects and those with alopecia areata, LCs were almost completely absent from the epidermis of scalps from subjects with lichen planopilaris (**Fig. 8b,c**). Although there are other possible explanations, these observations were

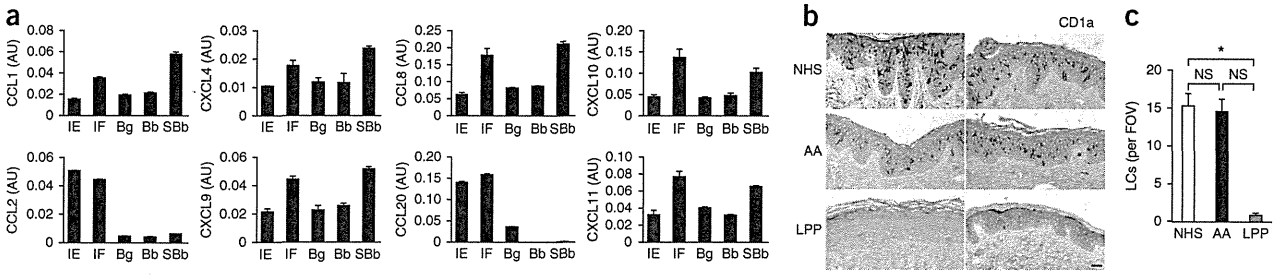

Figure 8 Chemokine expression in human hair follicles and LCs in hairless skin. (**a**) Real-time PCR analysis of the expression of mRNA for various chemokines (vertical axes; presented as in **Fig. 5c**) in human scalp tissues ($n = 2$ samples from one subject) dissected into the interfollicular epidermis (IE), infundibulum (IF), bulge (Bg), bulb (Bb) and suprabulb (SBb). (**b**) Immunohistochemistry of scalp sections from normal humans (NHS) and from patients with alopecia areata (AA) or lichen pilanopilaris (LPP), stained for CD1a ($n = 2$ samples per group). Scale bar, 20 μm. (**c**) Quantification of LCs in sections from **b** (as in **Fig. 7b**; pool of three fields of view per section and two sections per sample). Data are from one experiment representative of two independent experiments.

consistent with the proposal that the hair follicles are important portals for the entry of LCs into human epidermis.

DISCUSSION

Here we have shown that in response to mechanical perturbation or inflammation, pre-LCs arose from monomyeloid precursors that expressed LysM, showed CCR6 dependence and rapidly populated epidermis via hair follicles to differentiate into true LCs. Hair-follicle keratinocytes in the infundibulum and isthmus recruited LCs and pre-LCs via the production of CCL2 and CCL20, whereas $S1P_1^+$ suprabasal bulge cells negatively regulated repopulation by LCs via the production of CCL8. Pre-LCs failed to infiltrate the epidermis of hairless skin, which established mammalian hair follicles as portals for the entry of pre-LCs into the epidermis and as active participants in immunity.

CX3CR1-expressing cells give rise to LCs during embryonic development[18], and Gr-1^{hi} monocytes are reported to give rise to LCs in adult mice[17]. We did not detect eGFP on LCs and pre-LCs that arose from *Cx3cr1*$^{gfp/gfp}$ bone marrow[25]. We found that pre-LCs were immediate precursors of LCs that were derived from Gr-1^{hi} monocytes, but such LCs of monocytic origin represented only a subset of LCs in adult mice both in the steady state and in perturbed skin. Those rapidly repopulating pre-LCs of monomyeloid origin were distinct from the slowly expanding LC populations that appeared in the epidermis in clusters after conditional depletion[24], which bore all LC markers throughout repopulation[11].

We also considered the relationship of LCs and pre-LCs in the context of their use of chemokine receptors. In contrast to the effect of CCR2 deficiency on both LCs and pre-LCs, the effect of CCR6 deficiency was mainly on pre-LCs. Despite the lower abundance of CCR6-deficient pre-LCs, fully developed CCR6-deficient LCs were only slightly lower in abundance. Consistent with that, the generation of LCs and pre-LCs from LysM-DTA bone marrow showed that elimination of the LysM lineage resulted in the depletion of pre-LCs but did not result in fewer fully developed LCs to the same extent. Together with the finding that $LysM^{fm+}$ LCs represented only a subpopulation of LCs, these observations supported the proposal of at least two sources for LCs in adult mice. Although our data demonstrated that LCs of nonmonocytic origin also arose from the bone marrow, their exact origin(s) remain(s) to be clarified.

The association of LCs with hair follicles has been observed in human and mouse skin with undetermined importance[40,41]. Pre-LCs associated mainly with hair follicles before appearing in interfollicular epidermis, which led us to hypothesize that hair follicles might take part in recruiting DCs to the epidermis. Indeed, keratinocytes in the infundibulum and isthmus produced CCL20 and CCL2, respectively. Given the dependence of repopulation by LCs and pre-LCs on chemokine receptors, we propose that hair-follicle keratinocytes are the main sources of chemokines that recruit LCs and pre-LCs to the epidermis.

Notably, human hair-follicle keratinocytes also had distinct chemokine-expression profiles, which demonstrated that our findings obtained with mice also related to humans. Chemokine involvement has been linked to alopecia areata, in which T cells that attack hair follicles express CXCR3 (ref. 39), the receptor for CXCL4, CXCL9, CXCL10 and CXCL11 that we found were expressed by suprabulb keratinocytes. The suprabulb is probably responsible for the production of chemokines that recruit these pathogenic T cells.

We found that $S1P_1$ expression identified a distinct group of CCL8-producing suprabasal cells in the hair-follicle bulge, an immune-privileged area[4,5] that contains hair-follicle stem cells[1,42]. CCL8 expression by $S1P_1$ cells was induced after mechanical stress. It seems that the bulge is protected via the CCL8-CCR8 axis during repopulation by LCs and pre-LCs initiated by the infundibulum and the isthmus. $S1P_1$ is a regulator of the migration of T cells[33,34] and osteoclasts[35], as well as of angiogenesis[36]. It has been suggested that $S1P_1$-expressing endothelial cells must recruit vascular smooth-muscle cells to form tubules during angiogenesis. The effect of $S1P_1$ on chemokine-producing bulge cells remains to be addressed.

Mammalian hair has been regarded as a barrier that protects the body from a variety of physical stimuli, such as trauma, temperature changes and ultraviolet light, but an immunological function for hair has not been considered thus far, to our knowledge. External perturbation of this barrier could potentiate the entry of foreign materials and/or microorganisms, and it would pose considerable risk for the host should the immune system be unresponsive to such insults or unprepared for invasion. Skin is an organ that contains many leukocytes, with leukocyte numbers that exceed those in blood[43]. The recruitment and persistence of leukocytes in skin must therefore be tightly regulated. The regulation of DC trafficking by hair follicles seems to represent an important checkpoint, and hair follicles may control the intracutaneous distribution of other leukocytes. Our observations may have implications for the control of inflammation in skin diseases such as atopic dermatitis or psoriasis. Skin is also a major route for vaccination, and elucidating new mechanisms of regulating cells of the immune response in this leukocyte-epithelial interface may facilitate the percutaneous modulation of systemic immunity and thus enhance the development of new immunotherapies.

METHODS

Methods and any associated references are available in the online version of the paper.

Note: Supplementary information is available in the online version of the paper.

ACKNOWLEDGMENTS

We thank K. Eguchi and H. Ito for assistance, and M. Kajimura for assistance with multiphoton microscopy. Supported by the Japan Society for the Promotion of Science (K.N. and M.A.), The Kanae Foundation for the Promotion of Medical Science, and Japaneses Dermatological Association (K.N.), The Netherlands Organization for Scientific Research (B.E.C.) and the Intramural Research Program of the Center for Cancer Research of the National Cancer Institute (M.C.U.).

AUTHOR CONTRIBUTIONS

K.N. conceived of and designed all experiments; K.N. and T.K. did experiments, with the assistance of K.Mo., T.A., D.Y.M., S.U., K.H., M.O., A.K. and Y.C.; B.E.C. provided Langerin-DTR mice; K.Ma. provided bone marrow from mice deficient in CCR1, CCR2 or CCR5 and *Cx3cr1*$^{gfp/gfp}$ mice; G.C.F. and S.A.L. provided bone marrow from CCR8-deficient mice; J.M.F. provided bone marrow from CCR6-deficient mice; H.T., K.K. and M.S. assisted with multiphoton intravital microscopy; K.Mo. assisted with the sorting of hair-follicle keratinocytes; M.C.U. and M.A. interpreted data and guided the project; and K.N. and M.C.U. wrote the manuscript.

COMPETING FINANCIAL INTERESTS

The authors declare no competing financial interests.

Published online at http://www.nature.com/doifinder/10.1038/ni.2353.
Reprints and permissions information is available online at http://www.nature.com/reprints/index.html.

1. Cotsarelis, G., Sun, T.T. & Lavker, R.M. Label-retaining cells reside in the bulge area of pilosebaceous unit: implications for follicular stem cells, hair cycle, and skin carcinogenesis. *Cell* **61**, 1329–1337 (1990).
2. Lyle, S. *et al.* The C8/144B monoclonal antibody recognizes cytokeratin 15 and defines the location of human hair follicle stem cells. *J. Cell Sci.* **111**, 3179–3188 (1998).
3. Trempus, C.S. *et al.* Enrichment for living murine keratinocytes from the hair follicle bulge with the cell surface marker CD34. *J. Invest. Dermatol.* **120**, 501–511 (2003).
4. Christoph, T. *et al.* The human hair follicle immune system: cellular composition and immune privilege. *Br. J. Dermatol.* **142**, 862–873 (2000).
5. Meyer, K.C. *et al.* Evidence that the bulge region is a site of relative immune privilege in human hair follicles. *Br. J. Dermatol.* **159**, 1077–1085 (2008).
6. Hoek, R.M. *et al.* Down-regulation of the macrophage lineage through interaction with OX2 (CD200). *Science* **290**, 1768–1771 (2000).
7. Stefanato, C.M. Histopathology of alopecia: a clinicopathological approach to diagnosis. *Histopathology* **56**, 24–38 (2010).
8. Merad, M. *et al.* Langerhans cells renew in the skin throughout life under steady-state conditions. *Nat. Immunol.* **3**, 1135–1141 (2002).
9. Borkowski, T.A., Nelson, A.J., Farr, A.G. & Udey, M.C. Expression of gp40, the murine homologue of human epithelial cell adhesion molecule (Ep-CAM), by murine dendritic cells. *Eur. J. Immunol.* **26**, 110–114 (1996).
10. Bursch, L.S. *et al.* Identification of a novel population of Langerin+ dendritic cells. *J. Exp. Med.* **204**, 3147–3156 (2007).
11. Nagao, K. *et al.* Murine epidermal Langerhans cells and langerin-expressing dermal dendritic cells are unrelated and exhibit distinct functions. *Proc. Natl. Acad. Sci. USA* **106**, 3312–3317 (2009).
12. Borkowski, T.A., Letterio, J.J., Farr, A.G. & Udey, M.C. A role for endogenous transforming growth factor β1 in Langerhans cell biology: the skin of transforming growth factor β1 null mice is devoid of epidermal Langerhans cells. *J. Exp. Med.* **184**, 2417–2422 (1996).
13. Kaplan, D.H. *et al.* Autocrine/paracrine TGFβ1 is required for the development of epidermal Langerhans cells. *J. Exp. Med.* **204**, 2545–2552 (2007).
14. Zahner, S.P. *et al.* Conditional deletion of TGF-βR1 using Langerin-Cre mice results in Langerhans cell deficiency and reduced contact hypersensitivity. *J. Immunol.* **187**, 5069–5076 (2011).
15. Igyártó, B.Z. *et al.* Skin-resident murine dendritic cell subsets promote distinct and opposing antigen-specific T helper cell responses. *Immunity* **35**, 260–272 (2011).
16. Ouchi, T. *et al.* Langerhans cell antigen capture through tight junctions confers preemptive immunity in experimental staphylococcal scalded skin syndrome. *J. Exp. Med.* **208**, 2607–2613 (2011).
17. Ginhoux, F. *et al.* Langerhans cells arise from monocytes *in vivo*. *Nat. Immunol.* **7**, 265–273 (2006).
18. Chorro, L. *et al.* Langerhans cell (LC) proliferation mediates neonatal development, homeostasis, and inflammation-associated expansion of the epidermal LC network. *J. Exp. Med.* **206**, 3089–3100 (2009).
19. Mantovani, A., Bonecchi, R. & Locati, M. Tuning inflammation and immunity by chemokine sequestration: decoys and more. *Nat. Rev. Immunol.* **6**, 907–918 (2006).
20. Förster, R. *et al.* CCR7 coordinates the primary immune response by establishing functional microenvironments in secondary lymphoid organs. *Cell* **99**, 23–33 (1999).
21. Ohl, L. *et al.* CCR7 governs skin dendritic cell migration under inflammatory and steady-state conditions. *Immunity* **21**, 279–288 (2004).
22. Kabashima, K. *et al.* CXCL12-CXCR4 engagement is required for migration of cutaneous dendritic cells. *Am. J. Pathol.* **171**, 1249–1257 (2007).
23. Merad, M. *et al.* Depletion of host Langerhans cells before transplantation of donor alloreactive T cells prevents skin graft-versus-host disease. *Nat. Med.* **10**, 510–517 (2004).
24. Bennett, C.L. *et al.* Inducible ablation of mouse Langerhans cells diminishes but fails to abrogate contact hypersensitivity. *J. Cell Biol.* **169**, 569–576 (2005).
25. Auffray, C. *et al.* Monitoring of blood vessels and tissues by a population of monocytes with patrolling behavior. *Science* **317**, 666–670 (2007).
26. Cheong, C. *et al.* Microbial stimulation fully differentiates monocytes to DC-SIGN/CD209$^+$ dendritic cells for immune T cell areas. *Cell* **143**, 416–429 (2011).
27. Clausen, B.E., Burkhardt, C., Reith, W., Renkawitz, R. & Förster, I. Conditional gene targeting in macrophages and granulocytes using LysMcre mice. *Transgenic Res.* **8**, 265–277 (1999).
28. Kawamoto, S. *et al.* A novel reporter mouse strain that expresses enhanced green fluorescent protein upon Cre-mediated recombination. *FEBS Lett.* **470**, 263–268 (2000).
29. Mian, A. *et al.* Toxicity and adaptive immune response to intracellular transgenes delivered by helper-dependent vs. first generation adenoviral vectors. *Mol. Genet. Metab.* **84**, 278–288 (2005).
30. Jensen, U.B. *et al.* A distinct population of clonogenic and multipotent murine follicular keratinocytes residing in the upper isthmus. *J. Cell Sci.* **121**, 609–617 (2008).
31. Nagao, K. *et al.* Abnormal placental development and early embryonic lethality in EpCAM-null mice. *PLoS ONE* **4**, e8543 (2009).
32. Nishimura, E.K. *et al.* Dominant role of the niche in melanocyte stem-cell fate determination. *Nature* **416**, 854–860 (2002).
33. Matloubian, M. *et al.* Lymphocyte egress from thymus and peripheral lymphoid organs is dependent on S1P receptor 1. *Nature* **427**, 355–360 (2004).
34. Schwab, S.R. & Cyster, J.G. Finding a way out: lymphocyte egress from lymphoid organs. *Nat. Immunol.* **8**, 1295–1301 (2007).
35. Ishii, M. *et al.* Sphingosine-1-phosphate mobilizes osteoclast precursors and regulates bone homeostasis. *Nature* **458**, 524–528 (2009).
36. Liu, Y. *et al.* Edg-1, the G protein-coupled receptor for sphingosine-1-phosphate, is essential for vascular maturation. *J. Clin. Invest.* **106**, 951–961 (2000).
37. Horiuchi, K. *et al.* Conditional inactivation of TACE by a Sox9 promoter leads to osteoporosis and increased granulopoiesis via dysregulation of IL-17 and G-CSF. *J. Immunol.* **182**, 2093–2101 (2009).
38. Kobayashi, T., Iwasaki, T., Amagai, M. & Ohyama, M. Canine follicle stem cell candidates reside in the bulge and share characteristic features with human bulge cells. *J. Invest. Dermatol.* **130**, 1988–1995 (2010).
39. Ghoreishi, M., Martinka, M. & Dutz, J.P. Type 1 interferon signature in the scalp lesions of alopecia areata. *Br. J. Dermatol.* **163**, 57–62 (2010).
40. Gilliam, A.C. *et al.* The human hair follicle: a reservoir of CD40$^+$ B7-deficient Langerhans cells that repopulate epidermis after UVB exposure. *J. Invest. Dermatol.* **110**, 422–427 (1998).
41. Paus, R. *et al.* Generation and cyclic remodeling of the hair follicle immune system in mice. *J. Invest. Dermatol.* **111**, 7–18 (1998).
42. Ito, M. *et al.* Stem cells in the hair follicle bulge contribute to wound repair but not to homeostasis of the epidermis. *Nat. Med.* **11**, 1351–1354 (2005).
43. Clark, R.A. *et al.* The vast majority of CLA$^+$ T cells are resident in normal skin. *J. Immunol.* **176**, 4431–4439 (2006).

ONLINE METHODS

Mice. C57BL/6J mice and CAG-eGFP mice were from CLEA Japan. Langerin-DTR mice[6] were crossed to the C57BL/6 SJL (CD45.1$^+$) background and were maintained as heterozygotes. ROSA26-DTA, CCR1-deficient, CCR2-deficient and *Cx3cr1*$^{gfp/gfp}$ mice were from Taconic Farms or The Jackson Laboratory. Mice deficient in CCR5, CCR6 or CCR8 were generated as described[44–46]. LysM-Cre mice and CAG-CAT-eGFP mice have been described[27,28]. All mice were bred and housed in a pathogen-free environment. All animal procedures and study protocols were approved by the Keio University Ethics Committee for Animal Experiments.

Human tissue. Two sets of human scalp sample for gene analysis were obtained from excess normal skin that resulted from surgical removal of benign, subcutaneous skin tumors. Formalin-fixed, paraffin-embedded scalp sample from patients with alopecia were from biopsies obtained for diagnosis. All experimental procedures were officially approved by the Institutional Review Board and done in accordance with the ethical guidelines of Keio University. Human donors provided written informed consent in adherence to the Declaration of Helsinki Guidelines.

Preparation of epidermal sheets. Epidermal sheets were prepared as described[7]. Ears were split into dorsal and ventral halves with forceps, and only the ventral halves (with fewer terminal hairs) were used. Ear halves were incubated for 15 min on 3.8% ammonium thiocyanate (Wako Pure Chemical Industries) in phosphate buffer (pH 7.0). Epidermal sheets were manually detached from the dermis under a dissecting microscope. Sheets were fixed for 15 min at –20 °C in acetone or for 5 min at 25 °C in 4% paraformaldehyde (Wako Pure Chemical Industries) in PBS.

Preparation of epidermal cell suspensions. Epidermal cell suspensions were prepared from the whole trunk skin. Shaved trunk skin from mice was floated at 4 °C overnight on RPMI medium containing 0.25% trypsin and 0.27 mM EDTA. Epidermis was scraped off in complete RPMI medium, then was washed and filtered through a cell strainer (BD Falcon).

Antibodies. Monoclonal antibody to mouse EpCAM (G8.8; Developmental Studies Hybridoma Bank) was labeled with Alexa Fluor 488 or Alexa Fluor 647 (Invitrogen). Monoclonal antibody to mouse langerin (L31; eBioscience) were used in a purified or conjugated form, prelabeled with phycoerythrin (eBioscience) or labeled in-house with Alexa Fluor 488, Alexa Fluor 568 and Alexa Fluor 647 (Invitrogen). Additional antibodies used for immunofluorescence microscopy and flow cytometry included the following: antibody to MHC class II molecules I-A and I-E (M5/114.15.2), antibody to MHC class II molecule I-A^d (39-10-8), anti-CD11b (M1/70), anti-CD45 (30F-11), anti-CD45.1 (A20), anti-CD45.2 (104), anti-Gr-1 (RB6-8C5 and 1A8), anti-Ly6C (HK1.4), anti-F4/80 (BM8), anti-CD80 (16-10A1), anti-CD86 (GL-1), anti-CD135 (A2F10), anti-CD206 (C068C2), anti-CD1a (HI149) and anti-CD205 (NLDC-145; all from BioLegend); anti-B220 (RA3-6B2), anti-CD34 (RAM34), phycoerythrin-conjugated antibody to rat immunoglobulin G2a (R35-95), fluorescein isothiocyanate– or phycoerythrin-indotricarbocyanine–conjugated antibody to rat immunoglobulin G2b (RTK4530; all from BD Biosciences); anti-CCL1 (148107), anti-CCL2 (123616) and anti-CCL20 (114908; all from R&D Systems); anti-S1P$_1$ (PA1-1040; Thermo Scientific); anti–keratin 15 (CBL272; Millipore); and anti-CD11c (HL3; eBioscience). Primary antibodies were detected with the following secondary antibodies: Alexa Fluor–labeled goat anti-rat or anti-rabbit or anti–fluorescein isothiocyanate (A-11006, A-11077, A-21247, A-11011 and ANZ0202; all from Invitrogen). Mouse and rabbit antibodies were labeled with Zenon labeling kits (Invitrogen) where necessary. Antibody to mouse CD16-CD32 (93; BioLegend) was routinely used for blockade of Fcγ receptors before staining.

Immunofluorescence microscopy. Epidermal sheets and frozen skin sections were stained as described[11]. Sections or epidermal sheets were fixed in cold acetone for 2 min or 15 min, respectively, and were rehydrated three times in PBS for 5 min each. After blockade of Fc receptors with anti-CD16-CD32 (93; BioLegend), where appropriate, and blockade of nonspecific binding with 3% dry milk in PBS with 5% goat serum, for at least 1 h at 25 °C, primary antibodies were diluted in blocking buffer followed by incubation overnight at 4 °C. After washing, primary antibodies were detected with the appropriate Alexa Fluor–conjugated secondary antibodies (A-11006, A-11077, A-21247, A-11011 or ANZ0202; all from Invitrogen). Nuclei were visualized with Hoechst 33258 (Invitrogen). Both trunk skin and lower lip sections were prepared during pilot studies, but lip sections were routinely used because that allowed visualization of pilage hair and vibrissae, as well as oral mucosa. Images were obtained mainly with a Zeiss Axio Observer.Z1 with or without Apotome (Carl Zeiss), collected with the Axiovision software (version 4.8). Leica confocal microscope (TCS-SP5; Leica) was also used in some experiments. Photoshop CS 4 (Adobe) was used for adjustment where needed. Controls were treated identically throughout.

Immunohistochemistry. Antigen retrieval was done as described[31]. Formalin-fixed, paraffin-embedded tissue sections were deparaffinized and subjected to five 2-minute cycles of microwave treatment in citrate buffer (pH 6) and were allowed to cool to 25 °C. For sections subjected to antigen retrieval or frozen sections, nonspecific binding was blocked for 1 h at 25 °C with 3% skim milk (Morinaga) and 5% goat serum. Sections were incubated overnight at 4 °C with anti-CD1a (HI149; BioLegend) and then washed, and bound antibodies were detected with horseradish peroxidase–conjugated goat antibody to mouse immunoglobulin G (115-036-062; Jackson ImmunoResearch). Secondary antibodies were further visualized with a NovaRED Peroxidase Substrate Kit (Vector).

Flow cytometry and cell sorting. Data were collected with a FACSCanto II (BD Biosciences) and were analyzed with Flow Jo (Tree Star). Nonviable cells were excluded through the use of staining with 7-amino-actinomycin D (BioLegend) or propidium iodide (eBioscience), unless cells were fixed and permeabilized before analysis. Epidermal cells were sorted with a FACSAria II (BD Biosciences) directly into TRIzol LS (Invitrogen) and further processed for RNA extraction.

Depletion of LCs. Langerin-DTR mice received 1 μg DT (Sigma) in 200 μl PBS. In bone marrow–transfer experiments, recipient Langerin-DTR mice received DT 3 weeks after bone marrow transfer, as described below.

Generation of bone marrow chimeras. CD45.1$^+$ Langerin-DTR mice 6–8 weeks of age were lethally irradiated (950 rads delivered in a single dose) and then were injected intravenously with 2×10^6 total bone marrow cells from congenic mice. For evaluation of chemokine receptors in repopulation with precursors of LCs, bone marrow from wild-type C57BL/6 SJL (CD45.1$^+$) mice was transferred together with bone marrow from mice deficient in CCR1, CCR2, CCR5, CCR6 or CCR8, on the C57BL/6 J (CD45.2$^+$) background, at ratio of 1:1. Complete chimerism (≥95%) was confirmed by measurement of the frequency of B220$^+$ B cells in the blood 3 weeks after transplantation. For analysis of the relationship between Gr-1^{hi} monocytes and pre-LCs, CD115$^+$Gr-1^{hi} cells were isolated from bone marrow of LysM-eGFP mice and 5×10^6 cells were transferred into Langerin-DTR mice that had been irradiated with 4 Gy and treated with DT. Then, 1 week after topical application of 1% TNCB, epidermal ear sheets were collected for analysis.

Perturbation of ear skin. A solution of 1% TNCB (2,4,6-trinitro-1-chlorobenzene) in olive oil and acetone (1:3) in a volume of 20 μl was applied topically to the ventral sides of mouse ears, and 100 μl of 1% TNCB was applied topically to the dorsal skin to elicit inflammation in skin depleted of LCs to enhance repopulation with LCs. Tape stripping was done four times on the ventral side of mouse ears with Scotch tape, in which strips of tape were uniformly made to adhere to the ears and gently removed. A new strip of tape was used for each stripping procedure.

Isolation of human hair follicles. Human scalp samples were dissected into five fragments (interfollicular epidermis, infundibulum, isthmus, suprabulb and bulb) under a dissecting microscope (Leica) and were incubated overnight at 4 °C with 1,500 U/ml of Dispase II (Godo Syusei) in DMEM for removal of nonepidermal components.

Real-time PCR. Epidermal keratinocyte populations were sorted by flow cytometry and total RNA was purified with an RNeasy Micro Kit (QIAGEN). Then, cDNA was synthesized with SuperScript III First-Strand Synthesis SuperMix for qRT-PCR according to the manufacturer's protocol (Invitrogen). A Power SYBR Green PCR Master Mix (Applied Biosystems) and StepOne Real-Time PCR system (Applied Biosystems) were used for real-time PCR analysis. All primers (sequences, **Supplementary Table 1**.) were designed with Primer Express software (Applied Biosystems) and the following cycling conditions were used : 10 min at 95 °C, followed by 40 cycles of 15 s at 95 °C and 60 s at 60 °C. Expression of mRNA was normalized to the expression of GAPDH mRNA (encoding glyceraldehyde phosphate dehydrogenase) by the change in cycling threshold (ΔC_T) method and calculated based on $2^{-\Delta CT}$.

Multiphoton microscopy. Bone marrow from CAG-eGFP mice was transferred into lethally irradiated Langerin-DTR mice. At 8 weeks after transplantation, mice were depleted of LCs by treatment with DT. Mice underwent tape stripping of the inner ears 0.5–18 h before intravital observation. Images were observed and collected with a multiphoton microscope (FV1000MPE; Olympus)[47]. Mice were anesthetized by inhalation of isoflurane (Abbott). Images were analyzed with Imaris software version 6.3.1 (Carl Zeiss). In **Figure 4f,g** and **Supplementary Video 2**, $eGFP^+$ cells of interest were pseudocolored orange with Photoshop CS4 to distinguish them from irrelevant cells that also had high expression of eGFP.

Skin graft. Full-thickness skin obtained from *Adam17*$^{fl/fl}$*Sox9*-Cre mice and their wild-type littermates (I-A^b) within 3 weeks of birth was grafted onto opposite flanks of BALB/c (I-A^d) nude mice. Grafted skin was fixed with occlusive dressing for approximately 2 weeks. After graft establishment (at least 8 weeks), recipient mice were given topical application of 0.1% mometasone furoate ointment (Shionogi)[48] and topical treatment with 1% TNCB, followed by collection of samples for analyses 1 week later. Antibody to I-A and I-E (M5/114.15.2) was used for detection of $MHCII^+$ cells of either donor or recipient origin, and anti-I-A^d (39-10-8) was used for detection of those of recipient origin.

44. Chensue, S.W. *et al.* Aberrant in vivo T helper type 2 cell response and impaired eosinophil recruitment in CC chemokine receptor 8 knockout mice. *J. Exp. Med.* **193**, 573–584 (2001).
45. Hedrick, M.N. *et al.* CCR6 is required for IL-23-induced psoriasis-like inflammation in mice. *J. Clin. Invest.* **119**, 2317–2329 (2009).
46. Murai, M. *et al.* Peyer's patch is the essential site in initiating murine acute and lethal graft-versus-host reaction. *Nat. Immunol.* **4**, 154–160 (2003).
47. Morikawa, T. *et al.* Hypoxic regulation of the cerebral microcirculation is mediated by a carbon monoxide-sensitive hydrogen sulfide pathway. *Proc. Natl. Acad. Sci. USA* **109**, 1293–1298 (2012).
48. Belsito, D.V., Baer, R.L., Schultz, J.M. & Thorbecke, G.J. Relative lack of systemic effects of mometasone furoate on Langerhans cells of mice after topical administration as compared with other glucocorticosteroids. *J. Invest. Dermatol.* **91**, 219–223 (1988).

doi:10.1038/ni.2353

nature genetics

Genome-wide association study identifies eight new susceptibility loci for atopic dermatitis in the Japanese population

Tomomitsu Hirota[1], Atsushi Takahashi[2], Michiaki Kubo[3], Tatsuhiko Tsunoda[4], Kaori Tomita[5], Masafumi Sakashita[5], Takechiyo Yamada[5], Shigeharu Fujieda[5], Shota Tanaka[1,6], Satoru Doi[7], Akihiko Miyatake[8], Tadao Enomoto[9], Chiharu Nishiyama[10], Nobuhiro Nakano[10], Keiko Maeda[10], Ko Okumura[10], Hideoki Ogawa[10], Shigaku Ikeda[11], Emiko Noguchi[12,13], Tohru Sakamoto[14], Nobuyuki Hizawa[14], Koji Ebe[15], Hidehisa Saeki[16], Takashi Sasaki[17], Tamotsu Ebihara[17], Masayuki Amagai[17], Satoshi Takeuchi[18], Masutaka Furue[18], Yusuke Nakamura[19] & Mayumi Tamari[1]

Atopic dermatitis is a common inflammatory skin disease caused by interaction of genetic and environmental factors. On the basis of data from a genome-wide association study (GWAS) and a validation study comprising a total of 3,328 subjects with atopic dermatitis and 14,992 controls in the Japanese population, we report here 8 new susceptibility loci: *IL1RL1-IL18R1-IL18RAP* ($P_{combined} = 8.36 \times 10^{-18}$), the major histocompatibility complex (MHC) region ($P = 8.38 \times 10^{-20}$), *OR10A3-NLRP10* ($P = 1.54 \times 10^{-22}$), *GLB1* ($P = 2.77 \times 10^{-16}$), *CCDC80* ($P = 1.56 \times 10^{-19}$), *CARD11* ($P = 7.83 \times 10^{-9}$), *ZNF365* ($P = 5.85 \times 10^{-20}$) and *CYP24A1-PFDN4* ($P = 1.65 \times 10^{-8}$). We also replicated the associations of the *FLG*, *C11orf30*, *TMEM232-SLC25A46*, *TNFRSF6B-ZGPAT*, *OVOL1*, *ACTL9* and *KIF3A-IL13* loci that were previously reported in GWAS of European and Chinese individuals and a meta-analysis of GWAS for atopic dermatitis. These findings advance the understanding of the genetic basis of atopic dermatitis.

Atopic dermatitis is a chronic, relapsing skin disorder involving disturbed skin barrier functions, cutaneous inflammatory hypersensitivity and defects in antimicrobial immune defense with a strong genetic basis[1,2]. It is well established that common loss-of-function variants in *FLG* (encoding filaggrin) are a major predisposing factor for atopic dermatitis[3,4]. Association studies in populations of diverse ancestry, meta-analyses of studies and GWAS have shown that mutation in *FLG* is strongly associated with atopic dermatitis[4–7]. Apart from *FLG*, recent GWAS of European and Chinese populations for atopic dermatitis and a meta-analysis of GWAS have reported six susceptibility loci at a genome-wide level of significance—*C11orf30*, *TMEM232-SLC25A46*, *TNFRSF6B-ZGPAT*, *OVOL1*, *ACTL9* and *KIF3A-IL13*[5–7]. To gain a better understanding of the contribution of complex genetic effects to the pathogenesis of atopic dermatitis, it is important to identify additional susceptibility loci and validate the association of previously reported loci in different ancestry groups.

We performed a GWAS in the Japanese population with 1,472 individuals with atopic dermatitis (cases) and 7,971 controls using Illumina Human OmniExpress BeadChips (**Supplementary Table 1**). We subjected genotype data from a total of 606,164 SNPs to statistical analysis after principal-component analysis (PCA) and quality control filtering, and we generated a quantile-quantile plot using the Cochran-Armitage test (**Supplementary Fig. 1a–c**). The genomic inflation factor (λ_{GC}) was 1.03, indicating that there was a low possibility of false positive associations resulting from population stratification. The Manhattan plot showed that a total of 36 SNPs within 3 chromosomal regions at 2q12, 6p21.3 and 11p15.4 had associations that reached the genome-wide significance threshold of $P < 5 \times 10^{-8}$ (**Fig. 1**).

GWAS of European and Chinese populations and a meta-analysis of GWAS have reported seven susceptibly regions for atopic

[1]Laboratory for Respiratory Diseases, Center for Genomic Medicine, RIKEN, Yokohama, Japan. [2]Laboratory for Statistical Analysis, Center for Genomic Medicine, RIKEN, Minato-ku, Japan. [3]Laboratory for Genotyping Development, Center for Genomic Medicine, RIKEN, Yokohama, Japan. [4]Laboratory for Medical Informatics, Center for Genomic Medicine, RIKEN, Yokohama, Japan. [5]Department of Otorhinolaryngology, Fukui Medical University, Matsuoka, Japan. [6]Department of Otolaryngology–Head and Neck Surgery, University of Yamanashi, Faculty of Medicine, Chuo, Japan. [7]Osaka Prefectural Medical Center for Respiratory and Allergic Diseases, Habikino, Japan. [8]Miyatake Asthma Clinic, Osaka, Japan. [9]Nonprofit Organization (NPO) Japan Health Promotion Supporting Network, Wakayama, Japan. [10]Atopy Research Center, Juntendo University School of Medicine, Bunkyo-ku, Japan. [11]Department of Dermatology, Juntendo University School of Medicine, Bunkyo-ku, Japan. [12]Department of Medical Genetics, Majors of Medical Sciences, Graduate School of Comprehensive Human Sciences, University of Tsukuba, Tsukuba, Japan. [13]Japan Science and Technology Agency, Core Research for Evolutional Science and Technology (CREST), Saitama, Japan. [14]Division of Respiratory Medicine, Institute of Clinical Medicine, University of Tsukuba, Tsukuba, Japan. [15]Department of Dermatology, Takao Hospital, Kyoto, Japan. [16]Department of Dermatology, Jikei University School of Medicine, Minato-ku, Japan. [17]Department of Dermatology, Keio University School of Medicine, Shinjuku-ku, Japan. [18]Department of Dermatology, Graduate School of Medical Sciences, Kyushu University, Fukuoka, Japan. [19]Laboratory of Molecular Medicine, The Institute of Medical Science, The University of Tokyo, Minato-ku, Japan. Correspondence should be addressed to M.T. (tamari@src.riken.jp).

Received 27 April; accepted 11 September; published online 7 October 2012; doi:10.1038/ng.2438

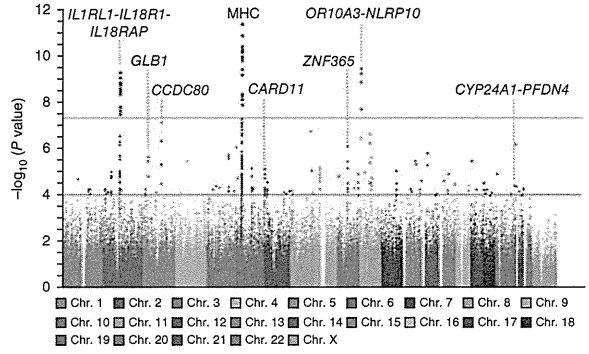

Figure 1 Manhattan plot showing the $-\log_{10}$ *P* values of 606,164 SNPs in the GWAS for 1,472 Japanese atopic dermatitis cases and 7,971 controls plotted against their respective positions on autosomes and the X chromosome. The red line shows the genome-wide significance threshold for this study ($P = 5 \times 10^{-8}$). The blue line shows the threshold ($P = 1 \times 10^{-4}$) for selecting SNPs for the validation study. Signals in the *IL1RL1-IL18R1-IL18RAP* (2q12), *GLB1* (3p21.33), *CCDC80* (3q13.2), MHC (6p21.3), *CARD11* (7p22), *ZNF365* (10q21.2), *OR10A3-NLRP10* (11p15.4) and *CYP24A1-PFDN4* (20q13) regions are indicated.

dermatitis[5–7]. We examined the previously reported regions in our GWAS and observed associations with atopic dermatitis for the SNPs in all of these regions (**Supplementary Fig. 2a–g** and **Supplementary Table 2**). Notably, the two regions identified in the previous GWAS of Chinese individuals had either the same SNP as the top signal in our study (20q13.3) or a SNP in strong linkage disequilibrium (LD) with the top SNP in the previous study (5q22.1); in contrast, for four of the five regions determined to be associated in Europeans, the top SNP in this study was in low LD with the previously reported best SNP.

To test for replication of the associations at the three loci suggested by the GWAS (2q12, 6p21.3 and 11p15.4) and to identify additional susceptibility loci for atopic dermatitis, we genotyped SNPs in a validation set consisting of a total of 1,856 individuals with atopic dermatitis and 7,021 controls (**Supplementary Table 1**). We first genotyped a total of ten tag SNPs ($r^2 < 0.80$) at the three loci and confirmed significant associations (**Supplementary Table 3**). We further investigated SNPs that showed *P* values of $<1 \times 10^{-4}$ in our GWAS and genotyped 87 tag SNPs ($r^2 < 0.80$) other than the previously reported loci and the three loci newly reported here. After Bonferroni correction with $P < 5.75 \times 10^{-4}$ (0.05/87), a total of 11 SNPs were found to be significantly associated with atopic dermatitis (**Supplementary Table 3**). We combined the data from the GWAS and

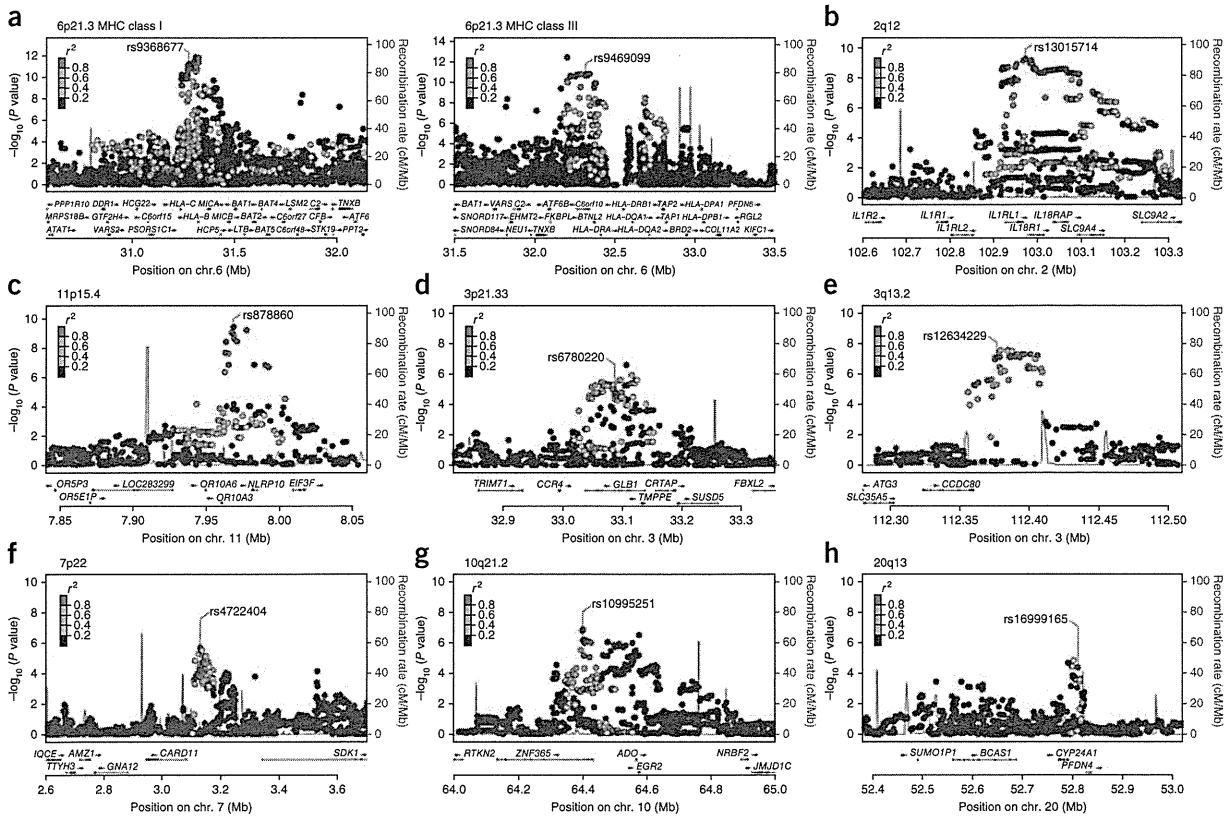

Figure 2 Regional plots of association results within eight newly identified susceptibility regions for atopic dermatitis. (**a–h**) Plots show the association results of both genotyped and imputed SNPs in the GWAS samples and the recombination rates within the susceptibility loci. For each plot, the $-\log_{10}$ *P* values (left *y* axis) of SNPs are shown according to their chromosomal positions (*x* axis). The genetic recombination rates are shown by the blue lines, and arrows indicate the locations of genes. The top genotyped SNP (labeled by rs number) is represented as a purple circle, and its LD (r^2) with the remaining SNPs is indicated by color. (**a**) MHC class I (left) and III (right) regions at 6p21.3. (**b**) 2q12. (**c**) 11p15.4. (**d**) 3p21.33. (**e**) 3q13.2. (**f**) 7p22. (**g**) 10q21.2. (**h**) 20q13.

Table 1 Summary of association results from the GWAS and validation study

SNP ID	Genes in or near regions of association	Chromosome (bp)	Allele (risk allele)	Stage	RAF		$P^{a,b}$	OR[b,c]	95% CI[b,c]	P_{het}[d]
					Case	Control				
rs13015714	*IL1RL1-IL18R1-IL18RAP*	2q12 (102971865)	T/G (G)	GWAS	0.473	0.412	5.17×10^{-10}	1.28	1.19–1.39	
				Validation	0.466	0.412	2.20×10^{-9}	1.25	1.16–1.34	
				Combined	0.470	0.412	8.36×10^{-18}	1.27	1.20–1.34	0.637
rs176095	*GPSM3* (MHC region)	6p21.3 (32158319)	T/C (T)	GWAS	0.860	0.811	3.86×10^{-10}	1.43	1.28–1.60	
				Validation	0.854	0.809	3.41×10^{-10}	1.38	1.25–1.53	
				Combined	0.856	0.810	8.38×10^{-20}	1.40	1.30–1.51	0.661
rs878860	*OR10A3-NLRP10*	11p15.4 (7968359)	A/G (G)	GWAS	0.603	0.540	3.47×10^{-10}	1.30	1.20–1.40	
				Validation	0.601	0.533	1.95×10^{-13}	1.32	1.23–1.42	
				Combined	0.602	0.537	1.54×10^{-22}	1.31	1.24–1.38	0.747
rs6780220	*GLB1*	3p21.33 (33087200)	T/G (G)	GWAS	0.582	0.539	1.55×10^{-5}	1.19	1.10–1.29	
				Validation	0.596	0.530	1.39×10^{-12}	1.31	1.21–1.41	
				Combined	0.590	0.535	2.77×10^{-16}	1.25	1.19–1.32	0.093
rs12634229	*CCDC80*	3q13.2 (112376308)	A/G (G)	GWAS	0.379	0.328	7.60×10^{-8}	1.25	1.15–1.36	
				Validation	0.391	0.326	8.18×10^{-14}	1.33	1.23–1.43	
				Combined	0.386	0.327	1.56×10^{-19}	1.29	1.22–1.37	0.303
rs4722404	*CARD11*	7p22 (3128789)	A/G (G)	GWAS	0.365	0.327	5.69×10^{-5}	1.18	1.09–1.28	
				Validation	0.362	0.325	2.67×10^{-5}	1.18	1.09–1.27	
				Combined	0.363	0.326	7.83×10^{-9}	1.18	1.12–1.25	0.911
rs10995251	*ZNF365*	10q21.2 (64398466)	T/C (C)	GWAS	0.568	0.518	7.73×10^{-7}	1.22	1.13–1.33	
				Validation	0.576	0.504	5.78×10^{-15}	1.34	1.24–1.44	
				Combined	0.572	0.511	5.85×10^{-20}	1.28	1.22–1.36	0.107
rs16999165	*CYP24A1-PFDN4*	20q13 (52807221)	T/C (T)	GWAS	0.729	0.691	3.87×10^{-5}	1.21	1.10–1.32	
				Validation	0.726	0.694	1.47×10^{-4}	1.17	1.08–1.27	
				Combined	0.728	0.692	1.65×10^{-8}	1.19	1.12–1.26	0.618

RAF, risk allele frequency; OR, odds ratio; CI, confidence interval.
[a]*P* values of the Cochran-Armitage trend test for each stage. [b]Results of combined analyses were calculated by the Mantel-Haenszel method. [c]Odds ratios and confidence intervals were calculated using the non-risk allele as a reference. [d]Results from the Breslow-Day test.

the validation set by the Mantel-Haenszel method, and a total of eight loci were found to be associated with atopic dermatitis at genome-wide significance (**Figs. 1** and **2** and **Table 1**). The Breslow-Day test showed an absence of significant heterogeneity ($P > 0.05$) (**Table 1**). We further assessed interactions among the eight newly discovered loci using the GWAS and validation data. We also conducted epistasis analysis, including the seven previously published loci, using the GWAS data. However, there was no evidence of an epistatic effect on susceptibility to atopic dermatitis with any combination of the 15 loci (**Supplementary Table 4**).

We obtained association results for >7 million imputed SNPs. In this study, a subset of genotype data for controls in the validation study was obtained from the GWAS data, but DNA samples were not available (**Supplementary Table 1**). Other cases and controls in the validation study were directly genotyped for SNPs at each locus. Thus, we focused on the directly genotyped SNPs in our GWAS and conducted a validation study. By imputation, we found that a total of 79 SNPs in 30 chromosomal regions were associated with atopic dermatitis at $5 \times 10^{-8} < P < 1 \times 10^{-4}$ (**Supplementary Table 5**). Further studies are needed to characterize the 30 regions suggested by imputation to associate with atopic dermatitis.

We next conducted conditional logistic regression analysis of the eight newly discovered loci using the GWAS data (**Supplementary Fig. 3**). This analysis indicated that there were two independent association signals in the MHC class I and III regions, one between *HLA-C* and *HLA-B* (rs9368677) and the other within *C6orf10* (rs9469099) (**Fig. 2a** and **Supplementary Fig. 3a**). In the *ZNF365* region, we observed independent signals at rs10995251, rs1444418 and rs10822056 (**Supplementary Fig. 3b**); however, the associations at rs1444418 and rs10822056 did not reach genome-wide significance when we combined the data from the GWAS and validation study ($P = 1.73 \times 10^{-7}$ and 1.15×10^{-4}, respectively). There were no independent signals in the other six associated regions (**Supplementary Fig. 3c–h**).

The associated region at 2q12 contains genes encoding the receptors of interleukin (IL)-1 family cytokines: *IL1RL1*, *IL18R1* and *IL18RAP* (**Fig. 2b** and **Table 1**). IL-1 family members are abundantly expressed in the skin[8]. IL1RL1, a component of the IL-33 receptor, is expressed by T helper type 2 (T_H2) cells and mast cells[9]. It has been reported that IL-33 is secreted in the damaged tissues of atopic dermatitis and promotes T_H2-type immune responses and the pathogenesis of atopic dermatitis[9]. The IL-1 receptor cluster region at 2q12 and the *IL33* region at 9p24.1 have also been identified as susceptibility loci by recent GWAS for bronchial asthma[10,11].

We found the most significant association with atopic dermatitis at rs176095 in the MHC class III region when we combined the data from the GWAS and validation study (**Fig. 2a** and **Table 1**). To our knowledge, this is the first finding of an association of atopic dermatitis with the MHC region at a genome-wide significance level. The MHC region is associated with a number of autoimmune diseases[12], and the involvement of autoimmunity in chronic inflammation in individuals with atopic dermatitis has been suggested[1]. Immunoglobulin E (IgE) antibodies against keratinocytes and endothelial cells are observed in serum specimens from subjects with severe atopic dermatitis[13].

The region of association at 11p15.4 includes two genes, *OR10A3* and *NLRP10* (**Fig. 2c** and **Table 1**). *OR10A3* is an olfactory receptor family gene, and *NLRP10* encodes a protein that belongs to the NALP protein family but lacks the leucine-rich repeat region. Individuals with atopic dermatitis are particularly susceptible to a number of microbial organisms, and pruritus is a major symptom of atopic dermatitis[1,2]. The itch-scratch cycle can lead to damage of the epidermal keratinocytes[1]. NLRP proteins are involved in sensing both microbial and danger signals[14], and NLRP10 has an anti-inflammatory

role through negative regulatory effects on caspase-1–dependent IL-1β secretion and apoptosis-associated speck-like protein containing a caspase recruitment domain (ASC)-mediated nuclear factor (NF)-κB activation[15].

The chromosome 3p21.33 region contains four genes, and the most significantly associated SNP, rs6780220, was located within *GLB1*, which encodes β-galactosidase-1 (**Fig. 2d** and **Table 1**). Notably, the associated region is located adjacent to the *CCR4* gene, which encodes a T_H2-associated chemokine receptor for CCL22 and CCL17 (also known as TARC). Keratinocyte-derived TSLP induces dendritic cells to produce TARC, and CCR4 mediates skin-specific recruitment of T cells during inflammation[1,16].

The associated region at 3q13.2 contains *CCDC80* (**Fig. 2e** and **Table 1**), which encodes a protein involved in the induction of C/EBPα and peroxisome proliferator-activated receptor γ (PPARγ)[17]. C/EBPα and C/EBPβ are coexpressed in basal keratinocytes and are upregulated when keratinocytes exit the basal layer and undergo terminal differentiation[18]. PPARγ acts as a negative regulator in immune cells, and a PPARγ agonist markedly suppresses both expression of thymic stromal lymphopoietin (TSLP) in the skin and maturation and migration of dendritic cells in a mouse model of atopic dermatitis[19].

The associated region at 7p22 contains *CARD11* (**Fig. 2f** and **Table 1**), which encodes CARMA1, an essential scaffold protein for lymphocyte activation via T-cell receptor (TCR) and B-cell receptor (BCR) signaling[20]. CARMA1 has an essential role in T-cell differentiation as well as a critical role in the regulation of the JunB and GATA3 transcription factors and the subsequent production of T_H2 cell–specific cytokines[21]. Mice that are homozygous for the mutation affecting Carma-1 show gradual development of atopic dermatitis with very high levels of serum IgE[22].

The region of association at 10q21.2 contains three genes, and the most significantly associated SNP, rs10995251, was located within *ZNF365* (**Fig. 2g** and **Table 1**). The region was reported to show suggestive association with atopic dermatitis ($P = 1.05 \times 10^{-7}$) by the previous GWAS of Chinese individuals[6], in which the association reached the genome-wide significance level. Notably, the region contains *EGR2*, which encodes a T-cell anergy-associated transcription factor that activates the expression of genes involved in the negative regulation of T-cell proliferation and inflammation[23].

The associated region at 20q13 includes *CYP24A1* and *PFDN4* (**Fig. 2h** and **Table 1**). *PFDN4* encodes a subunit of prefoldin, which is a molecular chaperone complex. *CYP24A1* encodes a mitochondrial cytochrome P450 superfamily enzyme. The protein initiates the degradation of 1,5-dihydroxyvitamin D3, the active form of vitamin D_3, by hydroxylation of the side chain[24]. Vitamin D is a modulator of innate and adaptive immune system functions[24], and an association between vitamin D deficiency and the severity of atopic dermatitis has been reported[25].

In this study, we identified variants at the *IL1RL1* and human leukocyte antigen (HLA) loci that associated with atopic dermatitis and replicated the associations at the *KIF3A-IL13* and *C11orf30* regions. The *C11orf30* region contains *LRRC32*, a gene previously reported to be specifically expressed in activated human naturally occurring regulatory T cells (nTreg)[26]. Atopic march is the natural history of atopic manifestations, and the clinical signs of atopic dermatitis generally predate the development of asthma and allergic rhinitis[27]. Recent GWAS have identified associations of the *IL1RL1*, HLA, *IL13* and *C11orf30* regions with bronchial asthma[10,11,28,29] and association of the *C11orf30* region with allergic rhinitis[30]. These findings suggest that atopic dermatitis and asthma or allergic rhinitis have overlapping susceptibility regions and that these regions contain common genetic factors for many allergic diseases. We stratified the cases by comorbidity of asthma and conducted an association study of asthma in the Japanese atopic dermatitis population for a total of 15 SNPs in the 7 previously reported and 8 newly identified regions. Notably, the most significant association was observed in the *IL1RL1* region ($P = 7.04 \times 10^{-9}$) (**Supplementary Table 6**).

In conclusion, we identified eight new susceptibility loci for atopic dermatitis at genome-wide significance, and we replicated the seven previously reported loci associated with atopic dermatitis in the Japanese population. Candidate genes at these loci suggest roles for epidermal barrier functions (*FLG* and *OVOL1*), adaptive immunity (*TNFRSF6B*, *IL13* and *CARD11*), IL-1 family signaling (*IL1RL1*, *IL18R1* and *IL18RAP*), negative regulation of apoptosis and the inflammatory response (*NALP10*), regulatory T cells (*LRRC32* and *EGR2*) and the vitamin D pathway (*CYP24A1*) in the pathogenesis of atopic dermatitis. Further studies are needed to better understand the genetic etiology and pathophysiology of atopic dermatitis.

URLs. The Leading Project for Personalized Medicine, http://biobankjp.org/; Haploview v4.2, http://www.broadinstitute.org/haploview/haploview; R statistical environment version 2.14.1, http://www.r-project.org/; minimac, http://genome.sph.umich.edu/wiki/Minimac; PLINK statistical software v1.07, http://pngu.mgh.harvard.edu/~purcell/plink/; LocusZoom, http://csg.sph.umich.edu/locuszoom/.

METHODS

Methods and any associated references are available in the online version of the paper.

Note: Supplementary information is available in the online version of the paper.

ACKNOWLEDGMENTS

We thank all the individuals who participated in the study and also thank the collaborating physicians for helping with sample collection. We are grateful to the members of BioBank Japan and the Rotary Club of Osaka-Midosuji District 2660 Rotary International in Japan for supporting our study. We thank M.T. Shimizu, H. Sekiguchi, A.I. Jodo, N. Kawaraichi and the technical staff of the Center for Genomic Medicine for providing technical assistance and K. Barrymore for proofreading this manuscript. This work was conducted as part of the BioBank Japan Project, which is supported by the Ministry of Education, Culture, Sports, Science and Technology, Japan. This work was also partly supported by grants from the Ministry of Health, Labour and Welfare, Japan.

AUTHOR CONTRIBUTIONS

T.H. and M.T. designed the study and drafted the manuscript. A.T. and T.T. analyzed the GWAS data. T.H., K.T., S. Tanaka and M.K. performed the genotyping for the GWAS. M.S., T.Y., S.F., S.D., A.M., T. Enomoto, C.N., N.N., K.M., S.I., K.O., H.O., E.N., T. Sakamoto, N.H., K.E., H.S., T. Sasaki, T. Ebihara, M.A., S. Takeuchi and M.F. recruited subjects and participated in the diagnostic evaluations. M.T. wrote the manuscript. M.K. and Y.N. contributed to the overall GWAS study design.

COMPETING FINANCIAL INTERESTS

The authors declare no competing financial interests.

Published online at http://www.nature.com/doifinder/10.1038/ng.2438.
Reprints and permissions information is available online at http://www.nature.com/reprints/index.html.

1. Bieber, T. Mechanisms of disease: atopic dermatitis. *N. Engl. J. Med.* **358**, 1483–1494 (2008).
2. Boguniewicz, M. & Leung, D.Y. Recent insights into atopic dermatitis and implications for management of infectious complications. *J. Allergy Clin. Immunol.* **125**, 4–13 (2010).
3. Palmer, C.N. *et al.* Common loss-of-function variants of the epidermal barrier protein filaggrin are a major predisposing factor for atopic dermatitis. *Nat. Genet.* **38**, 441–446 (2006).

4. Irvine, A.D., McLean, W.H. & Leung, D.Y. Filaggrin mutations associated with skin and allergic diseases. *N. Engl. J. Med.* **365**, 1315–1327 (2011).
5. Esparza-Gordillo, J. *et al.* A common variant on chromosome 11q13 is associated with atopic dermatitis. *Nat. Genet.* **41**, 596–601 (2009).
6. Sun, L.D. *et al.* Genome-wide association study identifies two new susceptibility loci for atopic dermatitis in the Chinese Han population. *Nat. Genet.* **43**, 690–694 (2011).
7. Paternoster, L. *et al.* Meta-analysis of genome-wide association studies identifies three new risk loci for atopic dermatitis. *Nat. Genet.* **44**, 187–192 (2012).
8. Johnston, A. *et al.* IL-1F5, -F6, -F8, and -F9: a novel IL-1 family signaling system that is active in psoriasis and promotes keratinocyte antimicrobial peptide expression. *J. Immunol.* **186**, 2613–2622 (2011).
9. Liew, F.Y., Pitman, N.I. & McInnes, I.B. Disease-associated functions of IL-33: the new kid in the IL-1 family. *Nat. Rev. Immunol.* **10**, 103–110 (2010).
10. Moffatt, M.F. *et al.* A large-scale, consortium-based genomewide association study of asthma. *N. Engl. J. Med.* **363**, 1211–1221 (2010).
11. Torgerson, D.G. *et al.* Meta-analysis of genome-wide association studies of asthma in ethnically diverse North American populations. *Nat. Genet.* **43**, 887–892 (2011).
12. Horton, R. *et al.* Gene map of the extended human MHC. *Nat. Rev. Genet.* **5**, 889–899 (2004).
13. Altrichter, S. *et al.* Serum IgE autoantibodies target keratinocytes in patients with atopic dermatitis. *J. Invest. Dermatol.* **128**, 2232–2239 (2008).
14. Magalhaes, J.G. *et al.* What is new with Nods? *Curr. Opin. Immunol.* **23**, 29–34 (2011).
15. Imamura, R. *et al.* Anti-inflammatory activity of PYNOD and its mechanism in humans and mice. *J. Immunol.* **184**, 5874–5884 (2010).
16. Vestergaard, C. *et al.* A Th2 chemokine, TARC, produced by keratinocytes may recruit CLA^+CCR4^+ lymphocytes into lesional atopic dermatitis skin. *J. Invest. Dermatol.* **115**, 640–646 (2000).
17. Tremblay, F. *et al.* Bidirectional modulation of adipogenesis by the secreted protein Ccdc80/DRO1/URB. *J. Biol. Chem.* **284**, 8136–8147 (2009).
18. Lopez, R.G. *et al.* C/EBPα and β couple interfollicular keratinocyte proliferation arrest to commitment and terminal differentiation. *Nat. Cell Biol.* **11**, 1181–1190 (2009).
19. Jung, K. *et al.* Peroxisome proliferator-activated receptor γ-mediated suppression of dendritic cell function prevents the onset of atopic dermatitis in NC/Tnd mice. *J. Allergy Clin. Immunol.* **127**, 420–429 (2011).
20. Hara, H. *et al.* Cell type–specific regulation of ITAM-mediated NF-κB activation by the adaptors, CARMA1 and CARD9. *J. Immunol.* **181**, 918–930 (2008).
21. Blonska, M. *et al.* CARMA1 controls Th2 cell–specific cytokine expression through regulating JunB and GATA3 transcription factors. *J. Immunol.* **188**, 3160–3168 (2012).
22. Jun, J.E. *et al.* Identifying the MAGUK protein Carma-1 as a central regulator of humoral immune responses and atopy by genome-wide mouse mutagenesis. *Immunity* **18**, 751–762 (2003).
23. Safford, M. *et al.* Egr-2 and Egr-3 are negative regulators of T cell activation. *Nat. Immunol.* **6**, 472–480 (2005).
24. Hart, P.H., Gorman, S. & Finlay-Jones, J.J. Modulation of the immune system by UV radiation: more than just the effects of vitamin D? *Nat. Rev. Immunol.* **11**, 584–596 (2011).
25. Peroni, D.G. *et al.* Correlation between serum 25–hydroxyvitamin D levels and severity of atopic dermatitis in children. *Br. J. Dermatol.* **164**, 1078–1082 (2011).
26. Wang, R. *et al.* Expression of GARP selectively identifies activated human $FOXP3^+$ regulatory T cells. *Proc. Natl. Acad. Sci. USA* **106**, 13439–13444 (2009).
27. Spergel, J.M. & Paller, A.S. Atopic dermatitis and the atopic march. *J. Allergy Clin. Immunol.* **112**, S118–S127 (2003).
28. Hirota, T. *et al.* Genome-wide association study identifies three new susceptibility loci for adult asthma in the Japanese population. *Nat. Genet.* **43**, 893–896 (2011).
29. Ferreira, M.A. *et al.* Identification of *IL6R* and chromosome 11q13.5 as risk loci for asthma. *Lancet* **378**, 1006–1014 (2011).
30. Ramasamy, A. *et al.* A genome-wide meta-analysis of genetic variants associated with allergic rhinitis and grass sensitization and their interaction with birth order. *J. Allergy Clin. Immunol.* **128**, 996–1005 (2011).

ONLINE METHODS

Study subjects. Characteristics of each case-control group are shown in **Supplementary Table 1**. All subjects with atopic dermatitis were diagnosed by physicians according to the criteria of Hanifin and Rajka[31]. All individuals were Japanese and gave written informed consent to participate in the study. This research project was approved by the ethical committees at the Institute of Medical Science, the University of Tokyo and the RIKEN Yokohama Institute.

BioBank Japan cases. The BioBank Japan project has been running since 2003, aiming at the collection of basic information for application to personalized medicine[32]. We selected case samples from the subjects who participated in the BioBank Japan, and a total of 1,472 cases for the GWAS and 940 cases for the validation study were recruited from several medical institutes, including the Fukujuji Hospital, Iizuka Hospital, Juntendo University, Hospital Iwate Medical University School of Medicine, National Hospital Organization Osaka National Hospital, Nihon University, Nippon Medical School, Shiga University of Medical Science, Cancer Institute Hospital of the Japanese Foundation for Cancer Research, Tokushukai Hospital and Tokyo Metropolitan Geriatric Hospital in Japan.

RIKEN cases. For the validation study, a total of 916 cases were recruited from the Takao Hospital, Kyushu University Hospital, University of Tokyo Hospital, Keio University Hospital, University of Tsukuba Hospital and several other hospitals.

BioBank controls. We used genome-wide screening data from subjects in the BioBank Japan project for the controls. Individuals with bronchial asthma and atopic dermatitis were excluded from the controls. Controls for the GWAS consisted of 6,042 cases in BioBank Japan with 1 of 5 diseases (cerebral aneurysm, esophageal cancer, endometrial cancer, chronic obstructive pulmonary disease and glaucoma), 1,023 healthy volunteers from members of the Rotary Club of Osaka-Midosuji District 2660 Rotary International in Japan[33] and 906 healthy subjects from the PharmaSNP Consortium.

A total of 5,547 cases registered in BioBank Japan with 1 of 4 diseases (epilepsy, urolithiasis, nephrotic syndrome and Graves' disease) were recruited for the validation study.

RIKEN controls. A total of 1,474 healthy volunteers were recruited from several medical institutes in Japan, including the Japanese Red Cross Wakayama Medical Center, Fukui University and Tsukuba University. Individuals with bronchial asthma and atopic dermatitis were excluded from the control group.

Genotyping and quality control. For the GWAS, we genotyped 1,491 cases and 7,983 controls using the Illumina Human OmniExpress BeadChip. We excluded a total of 19 cases and 12 controls because allele sharing analysis revealed that they were closely related, paired samples. We performed PCA of genotype data from the subjects along with data from European (CEU), African (YRI) and east Asian (Japanese (JPT) and Han Chinese (CHB) individuals obtained from the Phase 2 HapMap database by using smartpca[34]. The PCA plot indicated that cases and controls were genetically matched, with minimal evidence of population stratification (**Supplementary Fig. 1a,b**). We excluded samples with a call rate for autosomal SNPs of <0.98. We also excluded SNPs with minor allele frequencies of less than 0.01 from both cases and controls. SNPs having call rates of ≥99% in both cases and controls were used for the association study. We conducted exact Hardy-Weinberg equilibrium analysis, and SNPs with P values less than the cutoff value for the Hardy-Weinberg equilibrium test ($P < 1 \times 10^{-6}$ in controls) were excluded from the analysis.

In the validation study, we genotyped SNPs using the TaqMan assay (Life Technologies) or the multiplex PCR–based Invader assay (Third Wave Technologies). The genotype concordance rates for the eight SNPs in **Table 1** between samples genotyped using the Illumina Human OmniExpress BeadChip and those same samples genotyped with the TaqMan assay or multiplex PCR–based Invader assay were 1.000 and 1.000, respectively.

Statistical analysis. In the GWAS and validation study, the statistical significance of the association with each SNP was assessed using a 1-degree-of-freedom Cochran-Armitage trend test. We assessed association of SNPs on chromosome X by a meta-analysis with the Mantel-Haenszel method for two 2 × 2 allele frequency tables within male and female subjects. Odds ratios and confidence intervals were calculated from a 2 × 2 allele frequency table. We combined data from the GWAS and validation study by the Mantel-Haenszel method. Heterogeneity across the studies was examined using the Breslow-Day test[35]. Regional association plots were generated using LocusZoom[36].

Imputation. Imputation provides a high-resolution view of an associated region. Genotype imputation within the GWAS was performed using minimac. Association tests were performed with mach2dat using the fractional dosages output[37,38]. We used individuals from the 1000 Genomes Project (phased JPN, CHB and Han Chinese South (CHS) data, June 2011) as reference populations[39]. SNPs with a minor allele frequency of <5% and low quality of imputation ($r^2 < 0.7$) were excluded.

31. Hanifin, J.M. & Rajka, R.G. Diagnostic features of atopic dermatitis. *Acta Derm. (Stockholm)* **92** (suppl. 92), 44–47 (1980).
32. Nakamura, Y. The BioBank Japan Project. *Clin. Adv. Hematol. Oncol.* **5**, 696–697 (2007).
33. Takata, R. *et al.* Genome-wide association study identifies five new susceptibility loci for prostate cancer in the Japanese population. *Nat. Genet.* **42**, 751–754 (2010).
34. Price, A.L. *et al.* Principal components analysis corrects for stratification in genome-wide association studies. *Nat. Genet.* **38**, 904–909 (2006).
35. Breslow, N.E. & Day, N.E. Statistical methods in cancer research. Volume II—the design and analysis of cohort studies. *IARC Sci. Publ.* 1–406 (1987).
36. Pruim, R.J. *et al.* LocusZoom: regional visualization of genome-wide association scan results. *Bioinformatics* **26**, 2336–2337 (2010).
37. Li, Y. *et al.* MaCH: using sequence and genotype data to estimate haplotypes and unobserved genotypes. *Genet. Epidemiol.* **34**, 816–834 (2010).
38. Li, Y. *et al.* Genotype imputation. *Annu. Rev. Genomics Hum. Genet.* **10**, 387–406 (2009).
39. 1000 Genomes Project Consortium. A map of human genome variation from population-scale sequencing. *Nature* **467**, 1061–1073 (2010).